https://ntrs.nasa.gov/search.jsp?R=19790003804 2020-03-22T00:22:32+00:00

024

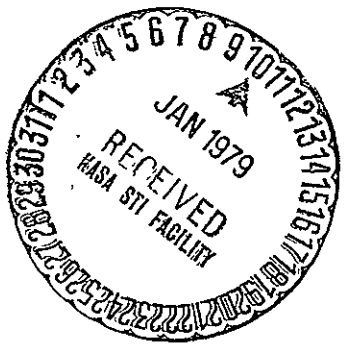

CORNELL UNIVERSITY

Center for Radiophysics and Space Research

ITHACA, N. Y.

(NASA-CR-157993) TEMPERATURE STRUCTURE AND EMERGENT FLUX OF THE JOVIAN PLANETS (Cornell Univ., Ithaca, N. Y.) 60 p HC A04/MF A01 CSCL 03B

N79-13975

Unclas
G3/91 40363

CRSR 707

TEMPERATURE STRUCTURE AND EMERGENT

FLUX OF THE JOVIAN PLANETS

Peter Silvaggio and Carl Sagan

TEMPERATURE STRUCTURE AND EMERGENT FLUX OF THE JOVIAN PLANETS

Peter Silvaggio*
and
Carl Sagan

Laboratory for Planetary Studies
Cornell University
Ithaca, New York 14853

October 1978

*Present Address: NASA Ames Research Center
Moffett Field, California 94035

A B S T R A C T

New long path, low temperature, moderate resolution spectra of methane and ammonia, broadened by hydrogen and helium, are used to calculate non-gray model atmospheres for the four jovian planets. Solar energy deposition in the upper atmospheres is of major importance; the fundamental and first overtone of hydrogen contributes enough absorption to create a thermal inversion for each of the planets. A wide range of models of emergent flux, dependent on assumed mixing ratios and scattering by condensates and photochemical organics, is used to calculate the suite of emergent spectral fluxes and representative limb darkenings and brightenings in the range 600 to 12,000 cm^{-1} for comparison with the Voyager infrared spectra. The temperature differences between jovian belts and zones corresponds to a difference in the ammonia cirrus particle radii (1 to 3 μm in zones; 10 μm in belts). The jovian tropopause is approximately at the 0.1 bar level. A thin ammonia cirrus haze should be distributed throughout the Saturnian troposphere; and NH_3 gas must be slightly supersaturated or ammonia ice particles carried upwards convectively in the upper troposphere of Saturn. Substantial methane clouds exist on both Uranus and Neptune, implying that considerable caution should be used in the application of simple reflecting models to interpret the spectroscopy of both planets. There is some evidence for almost isothermal structures

in the deep atmospheres of Uranus and Neptune. Expected seasonal variations during the Uranian year should be detectable in the emergent flux. There is either an internal heat source on Neptune or an abundance of particles with radii larger than 10 μm.

Silvaggio (1977) has described a new set of observations of the absorption of methane and ammonia in the infrared, using a multiple reflection folded path White cell with path lengths up to 72 m. Temperatures were varied between about 110° K and about 275° K and the effects of foreign gas band broadening by hydrogen and helium were studied over this temperature range. A subset of these observations at a resolution between 0.25 and 1.0 cm^{-1} measured over the spectral range 600 to 12,000 cm^{-1} lend themselves to the construction of model atmospheres and emergent fluxes for the four jovian planets, Jupiter, Saturn, Uranus and Neptune.

In order to reduce the number of frequency intervals needed for structure calculations, we used average monochromatic opacities (cf. Pollack, 1969). Because of atmospheric absorption in the visible and near infrared, each atmospheric layer has a non-zero absorption of solar energy and there will be a variation of the net flux with altitude. Effects due to the general circulation of the atmosphere are neglected. Our non-gray atmospheric models are based on the following additional assumptions: H_2, He, CH_4, NH_3 and possibly H_2O are the chief sources of infrared opacity. Scattering is approximated either by Rayleigh scattering or by Mie scattering for spherical particles. The atmosphere is in radiative equilibrium, except when the temperature gradient exceeds the adiabatic gradient, in which case the temperature gradient is set equal to the adiabatic gradient. The atmosphere is in hydrostatic equilibrium. The unsaturated components are completely mixed. The plane parallel atmosphere

approximation holds and the acceleration due to gravity is constant with altitude. The populations of the molecular energy levels are given by local thermodynamic equilibrium. The heat capacity of the atmosphere is large enough and the planetary rotation is fast enough that the effective temperature at a given latitude is independent of longitude. There is an opaque "surface," probably a sharp cloud deck, with a frequency-independent reflectivity. Saturated components, H_2O, NH_3, and CH_4, are assumed to form clouds, and the quantity of condensates is derived from the difference between the saturation vapor pressure and the partial pressure implied by the equation of hydrostatic equilibrium.

We solve the equation of radiative transfer iteratively. With an initial temperature profile and gas abundances for each constituent, a model atmosphere is generated, allowing for convection. The atmosphere is quantized, creating a finite number of layers and, for the purposes of radiation balance, a number of angles whose values are determined as those for Gaussian quadrature. For the conditions present in each layer, absorption and scattering coefficients are calculated and the equation of radiative transfer solved. The new temperatures derived in this manner replace the previous estimate, and the procedure then iterates until the temperature profile undergoes an arbitrarily small change. The emergent flux is constrained to equal the observed value. The temperature structure of the atmosphere is approximated by a series of layers, each of constant temperature T, for which the ideal gas law and the equation of hydrostatic equilibrium apply.

Some atmospheric constituents saturate as the temperature decreases; their densities can be approximated as $n_{sat} = (n_o/T) \exp [A - B/(T - C)]$, where the parameters have the values of Table 1.

Table 1

Gas	n_o $[cm^{-3}(K_o)^{-1}]$	Vapor Pressure Constants A	B	C	Temperature Range	Reference
NH_3	4.118×10^{17}	25.88	3752.6	-	all	Lasker (1963)
CH_4	9.673×10^{18}	16.5629	939.94	4.66	T < 60 K	Wilholt (1971)
		15.4172	933.61	5.38	60 K < T < 90K	
	7.35×10^{21}	-	-		T > 90 K	
H_2O	7.35×10^{21}	13.9787	5202.		T > 273 K	Handbook of Chemistry and Physics
		17.45915	6159.		T < 273 K	

When the temperature gradient exceeds the adiabatic gradient, the temperature gradient is set equal to the adiabatic gradient:

$$\left(\frac{dT}{dz}\right)_{ad} = -g/\bar{C}_p, \qquad \bar{C}_p = \sum_i n_i C_{p,i}/\Sigma n_i$$

where $C_{p,i}$ is the specific heat at constant pressure for gas i, and n_i is the density of gas i. Errors in $\bar{C}_p$ will be small (Dubisch, 1974) compared to errors in the ideal gas law. $C_{p,i}$ is calculated for each molecule by

$$C_p = c_1 + c_2 T + c_3 T^2 \text{ cal/deg-mole},$$

where the parameters have the values given in Table 2.

Table 2

Constants for Specific Heat

Gas	c_1	c_2	c_3	Reference
H_2	4.387	1.45×10^{-2}	-2.106×10^{-5}	Gopal (1966)
He	4.97	-	-	
CH_4	3.38	1.79×10^{-2}	-4.188×10^{6}	Zemansky (1957)
NH_3	5.92	8.96×10^{-3}	-1.764×10^{6}	
H_2O	6.89	3.28×10^{-3}	-0.343×10^{6}	

The value for H_2 is the specific heat for an equilibrium mixture (Trafton, 1965).

Where there is condensation, the adiabatic gradient can be derived from the Clausius-Clapyeron Equation, rewritten as

$$\left(\frac{dT}{dz}\right)_{ad} = -\frac{g}{C_p}\left[1 + \frac{H}{C_p T}\,\frac{m_c}{\bar{m}}\,\frac{n_c}{n}\left(\frac{m_c H}{kT} - 1\right)\right]$$

where H is the heat of vaporization/sublimation, C_p the average specific heat for the unsaturated gases, n_c the condensate number density, n the atmospheric number density, $\bar{m}$ the mean mass of atmospheric molecule, and m_c the mass of the condensing molecule.

The equation of radiative transfer is

$$dI_\nu/d\tau_\nu = I_\nu - J_\nu$$

where I_ν is the specific intensity, J_ν the mean intensity, and τ_ν the optical depth. Multiplying both sides by exp $(-\tau_\nu)$, integrating over τ_ν and assuming J_ν constant over an interval $\Delta\tau_\nu$, we find

$$I_\nu^{i+1} \simeq I_\nu^{i-1}\, e^{-2\Delta\tau_\nu} + (1 - e^{-2\Delta\tau_\nu})\ J_\nu^{-i} \qquad (1)$$

for the downward intensity at level i + 1, in terms of quantities at levels i and i - 1, each of optical thickness $\Delta\tau_\nu$. A similar relation applies for the upward intensity, I_ν^{i-1}. J_ν^{-i} is calculated by inserting the I_ν^i found in the previous step into the expression

$$J_\nu = \iint_\Omega P(\Omega) I_\nu d\Omega + \frac{\tilde{\omega}_o}{4} e^{-\tau_\nu} P(\Omega) I_o + (1 - \tilde{\omega}_o)\ B_\nu \qquad (2)$$

where $\tilde{\omega}_o$ is the single scattering albedo, B_ν is the Planck function, and I_o represents incident intensity. The phase function $P(\Omega)$ is constrained so that $\iint_\Omega P(\Omega) d\Omega = 4\pi$.

In the initial computation, the intensity is assumed to be zero in obtaining J. The downward intensity is first calculated beginning at the top of the atmosphere, and the calculations progress downward. Then, at reaching the bottom of the atmosphere, the upward intensity is calculated. This process is repeated, using the most recent estimates of I_ν^i, until I converges to a constant or slowly fluctuating value. The middle term in Eq. (2) is the source function due to the first scattering of the incident radiation. If this term becomes comparable to the others, then higher orders of scattering must be taken into account by adding the source function for higher orders of scattering

$$J_{n+1} = \frac{\tilde{\omega}_o}{4\pi} \left[\iint_\Omega P(\Omega) I_n d\Omega e^{-\tau} \right] \qquad \text{for } (n+1)^{th} \text{ order.} \qquad (3)$$

The working equation (2) and its analog for I_ν^{i-1} can be solved interatively. By adjusting the temperature of each level so that the radiation flux absorbed equals the flux reemitted, a temperature profile is derived. The correction to the temperature is $\Delta T \simeq (A-E)/4\sigma T^3$ where A is the flux absorbed, E the flux emitted, and σ the Stefan-Boltzmann constant. With an initial temperature guess for each layer, the program calculates a model atmosphere, then solves the equation of radiative transfer and makes a correction to the initial temperature estimate. On successive iterations the temperature corrections diminish until a solution is reached. We assume that only solar radiation is incident from above, and that the lower cloud surface is a partially reflecting layer at which some fraction of the incident energy is absorbed and the remainder reflected.

Trafton (1967) and Pollack and Ohring (1973) have previously calculated model atmospheres for Jupiter. We will employ our computational procedures to obtain improved atmospheric models, in particular by allowing for the temperature-dependence of the ammonia and methane opacity. The opacity of the pressure-induced transitions of hydrogen are determined essentially in the same manner as Trafton (1967). However, as Pollack and Ohring (1973) have done, we too allow for the deviation of the line profile in the far wings from a Lorentzian profile. Following a similar technique, the opacity due to the hydrogen fundamental vibrational and first overtone band is taken into account. Using the same method of calculation as Trafton, it is found that there is good

agreement (within 3%) with our observations of H_2 in the 500-1000 cm^{-1} range for 20 amagats of H_2 at temperatures of 120K, 195K, and 273K (cf. Fig. 1). Theory and observation for the first overtone band are compared in Fig. 2.

In general, ammonia has a broad opacity in the 8 - 14 μm range and dominates there, while hydrogen is the chief source of opacity between 14 and 40 μm, although there can be contributions from the pure rotation spectrum of water and ammonia. Methane dominates in the 6 - 8 μm range, and both methane and ammonia are strong sources of opacity shortward of 3.5 μm. The inclusion of methane and ammonia is important for Jupiter, while ammonia is of lesser importance for the other giant planets because their low effective temperatures prevent significant amounts of NH_3 from appearing in the upper layers. An entirely empirical expression for the self-broadening and foreign gas broadening as well as temperature dependence of methane and ammonia absorption, derived from the White cell measurements (Silvaggio, 1977), was used for the model atmospheres.

We have allowed in our calculations for Rayleigh scattering by the molecules in the free atmosphere and Mie scattering by the cloud aerosols. We approximate particles of arbitrary shape and composition by isotropic homogeneous spheres, because randomly oriented irregularly shaped particles should statistically approximate spherical symmetry (Sagan and Pollack, 1967). The spherical Bessel functions of Mie theory and their recursion relations were calculated by the method described by Wickramasinghe (1973). The gas amounts in the layers for our models

never exceeded by more than a factor of 2 the range of conditions run in the laboratory. Values of the absorption coefficient for methane at wavelengths shorter than 0.8 μm, important for calculating the solar energy deposition, were obtained from Giver (1978).

With a model identical to that in Pollack and Ohring (1973), this technique converged on a temperature profile that was virtually the same as their profile. Model atmospheres having the same properties but a different number of levels, frequency intervals or angles have been compared. A modest number of frequency intervals will provide an accurate model profile. However, the high spectral resolution for the emergent flux using the low resolution model profile is only as accurate as the low resolution temperature profile. For most cases, a modest number of layers, about 20, angles, about 12-16, and frequency intervals, approximately 100 cm^{-1} in width, give a model that is accurate to within 0.5^{o} K for each layer. The improvement by increasing the number of frequency intervals is due to a better averaging of the absorption coefficient over the interval, when weighted by the Planck function.

In nature, a distribution of particle size is usually encountered. If n(r)dr is the number of particles per unit volume with a radius between r and r + dr, the scattering efficiency becomes

$$Q_{sca} = \frac{K}{G} \int_{o}^{\infty} r^2 Q_{sca}(r) n(r) dr \Big/ \int_{o}^{\infty} r^2 n(r) dr, \qquad (4)$$

where G is the geometric cross-section of the particles. A similar expression for Q_{ext} applies for the extinction efficiency. For our calculations we use the distribution employed by Hansen (1971),

$$n(r) \propto r^{(1-3b)/b} \exp(-r/ab), \tag{5}$$

because it has simple properties and approximates several other distribution functions used in the literature, e.g. by Khrgian (1961) and Deirmendjian (1964). Figure 3 illustrates the distribution for several values of a and b.

The values of the index of refraction used for the gases were approximated with the Cauchy formula $n_r - 1 = \alpha(1 + \beta/\lambda^2)$, λ in μm, with coefficients given in Table 3.

TABLE 3

Cauchy Coefficients for Real Part of the Refractive Index of Gases

	α	β
H_2	13.58×10^{-5}	7.52×10^{-7}
He	3.48×10^{-5}	2.3×10^{-3}
CH_4	44.1×10^{-5}	-
NH_3	37.0×10^{-5}	1.2×10^{-3}
H_2O	2.5×10^{-4}	-

For particles we assumed n_r = 1.33 and 1.4, respectively, for H_2O and CH_4. These values do not take any dependence on temperature or wavelength into account. The H_2O clouds are deep in the troposphere of Jupiter and Saturn and should have little effect on energy balance. A complete treatment of H_2O can be found in Irvine and Pollack (1968). The CH_4 particles will be a significant factor on Uranus and Neptune, if there is condensation. However, no reliable data have been found for CH_4 particles in the middle infrared wavelengths. The values for the complex index of refraction of solid NH_3 were taken from Taylor (1973). These values were determined from a thin film of NH_3 at 77°K and do not account for any temperature dependence. However, the wavelength dependence has been resolved for 10 cm^{-1} intervals. For models employing the S_8/organic aerosol produced in Jovian simulation experiments by Khare and Sagan (1973), the values of $n(\lambda)$ were calculated assuming Mie scattering; the results should match their published spectrum at room temperature.

In the present study, a steady-state distribution of temperature and density for the atmosphere of a giant planet above an opaque surface has been calculated for a variety of models. The variables involved in such a study include the brightness temperature, gas abundances, spectral dependence of the albedo, and nature and location of Mie scatterers. With a very large number of possible combinations in a multi-dimensional phase space, and a finite budget, no attempt can be made to explore all effects on a fine grid. Rather, our approach is to develop a series of

models by successively adding an atmospheric constituent and examining its effects. We assume that, except for hydrogen, helium, methane, and ammonia (and ammonia and methane particles if condensation occurs), any other constituents will have an insignificant effect on the structure even though they may be noticeable in the emergent flux of the planet.

Our program does not require the specification of atmospheric temperatures at some lower boundary. Because our only constraint is the observed brightness temperature we do not explicitly postulate an internal heat source. In the case of Jupiter and Saturn, where the observed effective temperature is well above the temperature if there were no internal source, the temperature of the lower layers were increased until the calculated emergent flux equalled that observed. For Uranus and Neptune, where there is some doubt as to whether there is an internal heat source, the bolometric Bond albedo was chosen to be consistent with the effective temperature. The atmospheres of Uranus and Neptune at large optical depths may become isothermal below the CH_4 cloud (cf. Sagan, 1969). This effect can be altered by having larger CH_4 ice particles effectively scattering the long wavelength radiation.

Jupiter Atmospheric Structure

Jupiter is the nearest, brightest, closest and most visited of the outer planets, and is accordingly the best understood. Yet, there still exist uncertainties in the methane and ammonia abundances and there is a wide selection of minor constituents from which to choose. The

flights of Pioneers 10 and 11 (Carlson and Judge, 1974) and the β Scorpii occultation results (Elliot et al., 1974) indicate a helium abundance of approximately 10% and an effective temperature of 127° K (Orton, 1975a). The line of sight abundance of CH_4 is in doubt, with recent estimates ranging from 50 m-amagat (deBergh et al., 1976) to 250 m-amag (Lutz et al., 1976). Similarly the abundance of NH_3 ranges from 13 m-amagat (Mason, 1970) to 30 m-amagat (Woodman et al., 1977). The total abundance of H_2 seems to be 65 km-amagat (Margolis and Hunt, 1972; Fink and Belton, 1969). It is possible that the various amounts of CH_4 and NH_3, derived by observation of different bands and assuming a simple reflecting layer, are consistent if scattering is treated correctly.

Sagan and Salpeter (1976) have suggested a wide variety of possible particles in the troposphere of Jupiter. A worthwhile treatment of scattering requires an estimate of complex refractive indices, size distribution and number density. We shall assume that these particles will have little effect on the energy balance. However, they may be noticeable in the emergent flux. For the sake of definitiveness, the tropospheric particles will be assumed to be similar to the S_8/organic material synthesized by Khare and Sagan (1973, 1975). In addition, ethane is included with the absorption coefficients taken from Khanna et al. (1974). The size distribution for the particles [Eq. (5)] was arbitrarily but not implausibly chosen to be a = 1, b - 0.01.

Results on the Jovian atmospheric structure are shown in Figures 4 and 5 for the models of Table 4. The asymptotic temperature in the mesosphere is controlled almost exclusively by the abundance of methane. The minimum temperature at the top of the troposphere is controlled by the abundance of ammonia and the size of the NH_3-ice particles. The larger (10 μm) radii particles scatter the thermal radiation more effectively than the smaller (3 or 1 μm) particles. There is no noticeable difference between the 1 and 3 μm size particles in the resulting structure. No significant difference is found between Models 3 and 7.

The difference between belts and zones, while not explicitly explored, can be approximated by the large or small particle size models. If downward motion effectively removes the NH_3 cloud, the small particle radii models should accurately represent the cloud-free zones. The 4° K difference between Model 3 and Model 6 is of the same magnitude as the 3° K variation Orton (1975a) found between the South Tropical Zone and the South Equatorial Belt.

Also shown in Figure 4 are the model atmospheres of Orton (1975a) and Sagan and Salpeter (1976). The low temperature opacities derived in the laboratory raise the tropopause to approximately the 0.1 atm level, higher than in the other models. However, the Sagan and Salpeter model matches the present results reasonably well. The mesospheric temperatures in this work do not rise as quickly as those of Orton.

Table 4

Jupiter Model Atmospheres (cf. Figures 4 and 5)

	H_2	He	CH_4	NH_3	NH_3 Ice r_{avg}	T_e	
	km-amagat	km-amagat	m-amagat	m-amagat	(μm)	K	Other
1.	65	7.3	0	0	-	127	-
2.	65	7.3	50	0	-	127	-
3.	65	7.3	50	13	3	127	-
4.	65	7.3	250	13	3	127	-
5.	65	7.3	50	13	1	127	-
6.	65	7.3	50	13	10	127	-
7.	65	7.3	50	13	3	127	C_2H_6, Khare-Sagan material (2μm radius)

Saturn Atmospheric Structure

While the theoretical problems of the atmosphere of Saturn are similar to those for Jupiter, our knowledge of Saturn is much less extensive than that of Jupiter. H_2 was first identified on Saturn by Münch and Spinrad (1963). The common technique is the observation of the 4 - 0 and 3 - 0 overtones in the H_2 quadrupole spectrum. Abundances range from 190 km-amagat (Owen, 1969) to 80 km-amagat (Trafton, 1971). Recent estimates of methane abundances range from 35 m-amagat (Trafton, 1971) to 300 m-amagat (Lutz et al, 1976). The abundance of NH_3 on Saturn has been a matter of debate. A theoretical interpretation of the microwave spectrum of Saturn by Gulkis et al. (1969) requires NH_3; 2 m-amagat are obtained by Woodman et al. (1977). Whether there is enough ammonia to be detected by optical wavelength spectroscopy will depend upon details of the atmospheric structure. There are no definitive observations for the presence of helium. However, it seems unlikely that if helium is present its mixing ratio would differ greatly from that on Jupiter.

The infrared brightness temperature of Saturn has been measured and we shall use the broad-band measurement of Aumann et al. (1969) of 97° K as a representative value. If the bolometric albedo is 0.61, then this effective temperature implies that Saturn, like Jupiter, radiates more energy than it receives from the sun, about 3.5 times as much. (See also Erikson et al, 1978).

The model of atmosphere of Table 5 is exhibited in Figures 6 and 7. The addition of He or NH_3 warms Saturn's upper atmosphere only slightly, while CH_4 dramatically raises the temperature of the mesosphere. Because

TABLE 5

Saturn Model Atmospheres (cf. Figures 6 and 7)

	H_2 km-amagat	He km-amagat	CH_4 m-amagat	NH_3 m-amagat	NH_3 Ice r_{avg} (μm)	T_e °K
1.	100	0	0	0	-	97
2.	200	0	0	0	-	97
3.	100	25	0	0	-	97
4.	100	12.5	0	0	-	97
5.	100	12.5	35	0	-	97
6.	100	12.5	300	0	-	97
7.	100	12.5	100	0	-	97
8.	100	12.5	35	sat	3	97
9.	200	25	300	sat	3	97
10.	100	12.5	300	sat	3	93

of the low temperatures there can be little NH_3 in the upper atmosphere, so it is not unexpected that NH_3 contributes little to the absorption of sunlight. The amount of CH_4 affects the degree of warming, although the sensitivity to mixing ratio is not nearly so large as on Jupiter. These results are summarized in Table 6.

TABLE 6

Upper Atmospheric Temperatures on Saturn

(Maximum/Minimum °K)

H_2	73/70
He added	76/73
CH_4 (35 m-amagats)	112/75; with NH_3 113/75
CH_4 (100 m-amagats)	115/76
CH_4 (300 m-amagats)	121/81

All the models are consistent with a cloud deck in the 120 - 140° K range. When NH_3 is included, a thin NH_3-ice haze is distributed throughout the troposphere. The reflecting layer could be consistent with the top of the thicker portion of an NH_3 cloud. If the effective temperature of Saturn is as low as 93° K, then the reflecting layer is in the 110° K region. The upper atmosphere has a minimum of 70° K and warms to about 108° K.

Uranus and Neptune Atmospheric Structure

Hydrogen has been identified on Uranus and Neptune with the observation of the 3 - 0 and 4 - 0 bands. The abundances of H_2 are uncertain because of uncertainty about conditions under which the spectral lines are formed and the limited number of observations. Estimates range from 200 km-amagat by Poll (1971) to 500 km-amagat by Trafton (1974) for Uranus. Quadrupole lines at 1.4 μm have been reported on Neptune; the abundance above some high altitude is quoted as 5 km-amagat (Joyce et al., 1977). CH_4 has been observed and the range of abundances in 3 km - amagat by Owen (1967) to 15 km-amagat by Cess and Ramanathan (1972) for Uranus. Inhomogenous scattering models suggest the low end of this range (Macy et al., 1978). While estimates for CH_4 on Neptune (Danehy et al., 1978) are 15% more than on Uranus, the same mixing ratio implies the H_2 abundance to be a factor of 2 greater for Neptune. (See also Macy et al., 1978). Ammonia has not been identified in optical spectra of Uranus or Neptune, which is expected because of the low temperatures. There is no evidence on the presence or absence of He.

Only a limited number of brightness temperature measurements exist for these two outer planets. For the purpose of this paper, we shall adopt an equilibrium temperature of 58° K for Uranus and 48° K for Neptune (Danielson, 1977). The large 98° inclination of Uranus must result in severe seasonal changes. During 1966, the axis of Uranus was in the plane normal to the solar vector, while in 1985 the north pole will face the sun continuously. As a result, the effective temperature may then rise to 68° K assuming there is no effective heat exchange between hemispheres. With these low temperatures, methane clouds should form; for lack of a better estimate, the CH_4 ice size distribution function parameters will be taken as $a = 1$, $b = 0.01$.

The model atmospheres for Uranus and Neptune shown in Table 7 lead to the structures exhibited in Figures 8 and 9. Atmospheric temperatures near the 10 mb level are summarized in Table 8. An estimate of the possible long-term secular dependence of atmospheric structure on Uranus with orientation of the rotation axis can be garnered by comparing models 5 and 6 in Figure 8. The addition of helium and/or methane to the atmosphere results in a substantial warming of the upper portions of the atmosphere. However, extensive methane clouds must exist on both planets and it is impossible to attribute the large CH_4 absorption features to the gas above the reflecting layer. Most of the observed absorption must be the result of the cloud, either by multiple scattering and/or absorption by the methane ice itself. In the models considered, the clouds are extremely thick, with column densities > 50 g cm^{-2}, and it seems very plausible that the troposphere exhibits extensive multiple scattering. It is possible that the dramatic shallowing of the temperature gradients exhibited deep in the atmospheres of Uranus and Neptune represents an approach to isothermal deep atmospheres (in the absence of an internal heat source) as described by Sagan (1969). However, our calculation techniques are not designed for large optical depths and we do not here place extreme confidence in our deep atmosphere results.

TABLE 7

Uranus Models

	H_2 km-amagat	He km-amagat	CH_4 km-amagat	CH_4 ice $r_{avg}(\mu m)$	T_e ^oK
1.	250	0	0	-	58
2.	500	0	0	-	58
3.	250	28	0	-	58
4.	500	56	0	-	58
5.	250	28	sat	3	58
6.	250	28	10	3	68

Neptune Models

	H_2 km-amagat	He km-amagat	CH_4 km-amagat	CH_4 ice $r_{avg}(\mu m)$	T_e ^oK
1.	500	0	0	-	48
2.	500	56	0	-	48
3.	1000	0	0	-	48
4.	1000	120	0	-	48
5.	500	56	sat	3	48

TABLE 8

Upper Atmospheric Temperatures on Uranus and Neptune

(Maximum/Minimum °K)

	H_2	+He	+CH_4
Uranus	30/28	48/44	70/48
Neptune	25/23	30/27	60/39

The warm Uranus model appears very much the same as the nominal model, except that the troposphere is closer to the adiabatic lapse rate. For ice particles substantially larger than 3 μm, the contribution of the cloud becomes increasingly important because thermal radiation will no longer be able to penetrate a thick cloud.

Jupiter Emergent Flux

The modeling technique used for the solution of the radiative transfer problem in the atmospheres of the outer planets lends itself to the calculation of the brightness temperature as a function of wavelength and phase angle. The resolution of the infrared spectrum is limited only by the resolution of the absorption and scattering coefficients. Except for Jupiter, the outer planets have been observed primarily over broad band regions of the spectrum. By comparing the observed values with our calculated brightness temperatures, the range of parameters for the many variables can be narrowed. In this comparison, the resolution for the calculated brightness temperatures was kept approximately the same as for the observations. Below we propose a set of model parameters for each of the giant planets. However these form only a self-consistent set in agreement with the observations and do not necessarily exclude other models involving a different set of assumptions.

Figure 10 displays three sets of data in the 7 to 14 μm window in the Earth's atmosphere for Jupiter, compared with the calculated emergent fluxes for Jupiter Models 3 and 4 of Table 4. It immediately follows that the abundance of CH_4 above the reflecting layer must be $\sim$ 150 - 200 m-amagat. Model 3 (50 m-amagat of CH_4) is clearly too cold in the 8 - 14 μm region, while Model 4 (250 m-amagat of CH_4) is marginally acceptable, but slightly on the warm side. Encrenaz et al. (1976) have measured this region with a resolution of $\sim$10 cm^{-1} and found the ν_4 band of CH_4 to appear as an emission feature with a temperature of $\sim 145^{\circ}$ K. This value agrees quite well with other observations and supports a

CH_4/H_2 mixing ratio of $\sim 2 \times 10^{-3}$ which is the value Orton (1975b) proposes. The lower abundances of CH_4 derived by de Bergh et al. (1976) for the $3\nu_3$ band of CH_4 perhaps should be re-examined especially with regard to the placement of the continuum.

Other model comparisons suggest that the ammonia particle radius is $\sim$ 3 μm or smaller, which agrees with Kawata and Hansen (1976) who found the particles to be less than 2 μm. The larger radii model depressed the brightness temperature in the 9 - 12 μm region approximately 2° K, while the 1-μm-sized particles had little effect in this region.

The thermal radiation (15 - 40 μm) calculated in Figure 11 also supports the 150 m-amagat CH_4 model. Model 4 is seen to be slightly warmer than the observed values, although not significantly greater than the spectrum of Houck et al. (1975). From this comparison we find that one suitable model atmosphere which seems to be consistent with all of the data we have presented is that displayed in Table 9. As mentioned earlier, there could conceivably be a wide range of other comparably acceptable atmospheric models which match the data equally well.

The effect of phase angle was studied briefly (Figure 12). The ν_4 band of CH_4 shows almost no variation from center to limb, while the ν_2 band of NH_3 shows a definite limb brightening. The broad band, 10 - 20 μm, was found to exhibit limb brightening as was observed with Pioneer 10 and 11 (Orton, 1975a).

TABLE 9

An Acceptable Jovian Model Atmosphere

H_2	$\sim$65 km-amagat
He/H_2	0.125
CH_4	$\sim$150 m-amagat; CH_4/H_2 $\sim 2 \times 10^{-3}$
NH_3	$\sim$13 m-amagat; NH_3/CH_4 $\sim$1/3, deep in the troposphere
NH_3 Ice	$\lesssim$3 μm radii
T_e	$\sim 127^{\circ}$ K

Sagan and Salpeter (1976) have proposed a variety of molecular and aerosol constituents in the jovian atmosphere. Our models, with T_B $\sim 200^{\circ}$ K in the 5 μm region, are quite consistent with a dense reflecting layer cloud at $\sim 200^{\circ}$ K, which is the appropriate level for a NH_4SH cloud. They have suggested ethane, C_2H_6, with a mixing ratio $\sim 5 \times 10^{-7}$. Also suggested are complex organic molecules/particles that reside in the lower troposphere, below the NH_3 cloud. Our Model 7 has attempted a cursory examination of these two additional atmospheric constituents. The C_2H_6/H_2 ratio was 5×10^{-7} and the complex organic particles were assumed to reside in the layer below the NH_3 cloud base and have an average radius of 3 μm.

The spectral characteristics were approximated by Khanna et al. (1974) for C_2H_6 and Khare and Sagan (1973) for the S_8/organics. The emergent flux was essentially unchanged except for the ν_9 C_2H_6 band in emission with $T_B \sim 120^\circ$ K without C_2H_6. This would correspond to $T_B \sim 135^\circ$ K for the higher methane abundance model. We were unable to discern any significant difference in the 8 - 14 μm region with the addition of the complex organic particles. This is due to two effects: (1) their absorption features are masked by higher level CH_4 and NH_3, and (2) any scattering is also masked by the overlying NH_3 cloud. The 8 - 14 μm region does not seem to be the optimum region for such observations.

Saturn Emergent Flux

In comparing the calculated and observed brightness temperatures of Saturn (Fig. 13), it is evident that there are areas both of good and poor agreement. The models all compare favorably with Low and Davidson (1969) in the 5 μm region, with $T_B \sim 120^\circ$ K being essentially the NH_3 cloud top. Similarly, good agreement is found in the 20 μm region. The major problem is in the 8 - 14 μm portion of the spectrum, where NH_3 and NH_3-ice particles play an important role.

The spectra for Models 7 and 9 (100 m-amagat of CH_4) fall between the spectra of Models 5 and 6 (35 and 300 m-amagat of CH_4, respectively). The only difference the addition of NH_3 made was the lowering of the brightness temperature by several degrees in the 8 - 12 μm region. However, the models are still almost 10°K too warm in this region [cf. $93 \pm 3^\circ$K for 8 - 14 μm (Low, 1964) and $99 \pm 8^\circ$K for 10 μm (Murphy et al., 1972)].

In order to match these observations, there must be a mechanism that provides more NH_3 to the upper reaches of the troposphere. There are at least two possible such mechanisms: (1) NH_3 is slightly supersaturated or (2) convection carries the NH_3-ice particles to higher altitudes. A first order estimate of the NH_3 required is only about a factor of 2 more than is present in Model 9 in agreement with Woodman et al. (1977).

The emergent flux in the narrow spectral region of 1280 - 1330 cm^{-1} is virtually independent of phase angle (see Fig. 14). The band centered on the methane fundamental at 1306 cm^{-1} had a brightness temperature equal to the asympotic mesospheric temperature of the model. An observation in this region of the spectrum would give a fairly accurate estimate of the CH_4 abundance on Saturn. The low NH_3 abundance should be seen in a 920 - 970 cm^{-1} limb darkening. The 10 - 20 μm broad band is also seen to darken as the limb is approached. If there is a mechanism for pumping NH_3 into the upper troposphere of Saturn, it should affect the limb darkening in the 8 - 14 μm region, perhaps even reversing the limb darkening to brightening.

The evidence is insufficiently clear to refine our estimates of hydrogen and methane abundances beyond the range our models covered. A measurement of the brightness temperature in the 1300 cm^{-1} region should give a reliable asympotic value for the mesospheric temperature. From this value, the abundance of methane can be deduced. The effective temperature of 97° K seems to fit the observations quite well, with T_e = 93° K being clearly too cold. Consequently, Saturn, like Jupiter, must have an internal heat source that provides approximately 3.5 times as much energy as Saturn receives from the sun.

Uranus and Neptune Emergent Flux

The paucity of observations of Uranus and Neptune rule out definitive conclusions at present. This is also true because our models indicate substantial methane clouds on both planets. Our understanding of scattering by CH_4-ice particles is limited to that of non-absorbing Mie scatterers of unknown size or distribution. The large abundances reported for H_2 and CH_4 are an overestimate unless our saturation vapor pressure curve for methane has substantial errors at the low temperature extremes found on these planets. Absorption features seen in the visible and near infrared portions of the spectrum must be greatly enhanced by multiple scattering.

In our models, the average particle radius was 3 μm; this size does not seriously effect the long wavelength thermal radiation. If the CH_4-ice particles are larger, then the shorter wavelength thermal radiation will originate higher in the atmosphere, making it cooler, the troposphere will warm and the longer wavelength radiation will appear at higher temperatures. A comparison of theory and observation for Uranus is displayed in Figure 15. An example of an acceptable model atmosphere for Uranus and for Neptune is displayed in Table 10. Our Model 5 for Uranus matches the observations rather well and it would seem fairly easy to detect a rise in the planet's effective temperature, if it is subject to seasonal variations.

The spectrum of Neptune (see Fig. 16) with an effective temperature of 48° K clearly appears too cold. The S(0) and S(1) lines of the pressure induced hydrogen transitions are formed near the top

of the thick methane cloud. If the amount of methane was not forced to be maximized, the cloud top would be lower and the effective temperature would be higher. A T_e of roughly 52° K would give a better match to the observations. However, this would require an internal heat source for Neptune, as has been suggested by Murphy and Trafton (1974). An alternative could be larger size scatterers. The 10 μm radius particles were seen to raise the tropospheric temperature on Jupiter, and the same effect should take place on Neptune. This will raise the brightness temperatures of the longer wavelength radiation at the expense of the shorter radiation, which would improve the agreement between the observed and calculated brightness temperatures for wavelengths greater than 20 μm. A measurement of T_B at a wavelength < 20 μm is very important for Neptune, and would distinguish between either large particle scatterers or an internal heat source.

With the extensive methane cloud deck, it makes little sense to talk of simple reflecting layer models. There appears to be only about 10% of the observed amounts of H_2 above the cloud deck and the CH_4/H_2 mixing ratio is governed by the saturation vapor pressure curve in the troposphere and by the temperature minimum in the mesosphere.

TABLE 10

Acceptable Uranian and Neptunian Model Atmospheres

	Uranus	Neptune
H_2 above CH_4 cloud tops	7 km-amagat	10 km-amagat
He/H_2	0.125	0.125
CH_4/H_2 in mesosphere	$\sim 2 \times 10^{-5}$	$\sim 3 \times 10^{-7}$
T_e	58° K	$\sim 48^{\circ}$ K with large particles
		$\sim 52^{\circ}$ K with small particles

CONCLUSIONS

The new methane and ammonia laboratory measurements and the modeling techniques described here have a range of applications beyond those of the present paper, including a more thorough study of the brightness temperature in the 5 to 25 μm region and an exploration of the consquences of a very large amount of methane on Uranus and Neptune as proposed by Danielson (1977). This exploration has underscored the importance of better understanding the complex refractive indices of methane and ammonia in the infrared, and of using more realistic band formation models in estimating atmospheric abundances, especially for Uranus and Neptune, where much of the observed gas opacity must be due to multiple scattering in the methane clouds. A range of new observations, for example, broad band brightness temperature measurements for Neptune short of 20 μm, can play an important role in distinguishing among competing models. In particular the results presented here may be of use in the analysis of limb darkening (or brightening) and measurements of the emergent spectral flux from Jupiter and Saturn (and possibly from Uranus) in the Voyager missions.

ACKNOWLEDGMENTS

This research was supported by the Planetary Atmospheres program of the National Aeronautics and Space Administration under Grant NGR 33-010-082. We are grateful to Robert W. Boese for the use of his White cell laboratory in which the spectrometric measurements were made and for his support of these studies; to J.B. Pollack and L.P. Giver for helpful discussions, and to J. McGee, J. Morgan, W. Kyle, G. Coon, D. Hafeman, J. Magalhaes, D. Meckfessel and A. Aurelius for laboratory, numerical processing and other assistance.

Figure Captions

Figure 1. Laboratory spectra of 21 amagats of H_2 at 331 cm path length. The two spectra shown are for temperatures of 195° K and 120° K, at a 0.5 cm^{-1} resolution. The two absorption lines in the 900 cm^{-1} region are due to trace amounts of NH_3 in the cell. The calculation of the transmission based on Trafton's (1967) technique falls within the noise level of the spectra.

Figure 2. A comparison of previously published H_2 spectra and our calculation for the first overtone band.

Figure 3. Size distribution from Eq. (5) for two values of a and three values of b (Hansen and Travis 1974).

Figure 4. Temperature profiles for model atmospheres of Jupiter. (The numbers on the curves correspond to those of the models in Table 4.)

Figure 5. Temperature profiles for model atmospheres of Jupiter for different aerosol particle sizes. Model 3 (3 μm mean radius) and Model 5 (1 μm mean radius) are essentially identical, while Model 6 (10 μm mean radius) is warmer.

Figure 6. Temperature profile for model atmospheres of Saturn for $T_e = 97°$ K. (The numbers on the curves correspond to the numbers of the models in Table 5.)

Figure 7. Temperature profiles for model atmospheres of Saturn for $T_e = 93°$ K.

Figure 8. Temperature profiles for Uranus model atmospheres. (The numbers on the curves correspond to the numbers of the models in Table 7.)

Figure 9. Temperature profiles for Neptune model atmospheres. (The numbers on the curves correspond to the numbers of the models in Table 7.)

Figure 10. Calculated brightness temperatures for model atmospheres of Jupiter in the 7 - 14 μm region of the spectrum. Model 3 invokes small methane abundances, Model 4 much larger ones. The models are compared to three sets of observations as shown. Resolution is ∿0.2 μm, or ∿20 cm^{-1}.

Figure 11. Calculated brightness temperatures for model atmospheres of Jupiter in the 100 - 900 cm^{-1} region. Observations are as follows: (a) Low (1965); (b) Harper et al. (1972); (c) Armstrong et al. (1972); (d) Low et al. (1973); (e) Aitken and Jones (1972); (f) Gillett et al. (1969); (g) Chase et al. (1974); (h) Wright (1976). Curves are for small (50 m-amagat) and large (250 m-amagat) amounts of CH_4, with and without NH_3.

Figure 12. Limb brightening/darkening of Jupiter for various spectral regions based on Model 4 and compared with the results of Orton (1975a).

Figure 13. Calculated brightness temperatures for Saturn are displayed for Model numbers 5, 6, 8 and 10 summarized in Table 5. The wide band-pass temperatures are indicated by the horizontal lines for Model 5 and dashed lines for Model 6. Additional data are from (i) Nolt (1977); and (j) Ward (1977).

Figure 14. Limb brightening/darkening of Saturn for various spectral regions based on Model 9.

Figure 15. Spectra of Uranus from Rieke and Low (1974) [error bar with arrow], with data added from Murphy and Trafton (1974), Low (1966), [error bar at 500 cm^{-1}] and Gillett and Rieke (1977) boxes. Also shown are the calculated brightness temperatures for the H_2, He, and CH_4 models of Uranus: (Model 5) $T_e = 58^{\circ}$ K, (Model 6) $T_e = 68^{\circ}$ K, summarized in Table 7. The wide band-pass calculation are indicated by the horizontal dashed lines.

Figure 16. Spectra of Neptune from Rieke and Low (1974) [boxes] with Murphy and Trafton (1974) [error bar at 500 cm^{-1}] and Gillett and Rieke (1977) [error bar with arrow] data added. Also shown are the calculated brightness temperature for the H_2, He, and CH_4 model of Neptune; $T_e = 48^{\circ}$ K. The wide band-pass calculations are indicated by the horizontal dashed lines.

References

Aitken, D. K., and Jones, B. (1972) The 8 - 13 μm Spectrum of Jupiter, Nature 240, 230-232.

Armstrong, K. R., Harper, D. A., Jr., and Low, F. J. (1972), Far-Infrared Brightness Temperatures of the Planets, Astrophys. J. 178, L89-L92.

Aumann, H. H., Gillespie, C. M., Jr., and Low, F. J. (1969) The Internal Powers and Effective Temperatures of Jupiter and Saturn, Astrophys. J. 157, L69-L72.

Carlson, R. W., and Judge, D. L. (1974) Pioneer 10 Ultraviolet Photometer Observations at Jupiter Encounter, J. Geophys. Res. 79, 3623-3633.

Cess, R. D., and Ramanathan, V. (1972) Radiative Transfer in the Atmosphere of Mars and that of Venus Above the Cloud Deck, J.Q.S.R.T. 12, 933-945.

Danehy, R.G., Owen, T., Lutz, B.L., Woodman, J.H., (1978) Detection of the Kuiper Bands in the Spectrum of Titan, Icarus 35, 247 - 251.

Danielson, R. E. (1977) Structure of the Atmosphere of Uranus, Icarus 30, 462-478.

de Bergh, C., Maillard, J. P., Lececheux, J., and Combes, M. (1976) A Study of the $3\nu_3$ - CH_4 Region in a High-Resolution Spectrum of Jupiter Recorded by Fourier Transform Spectroscopy, Icarus 29, 307-310.

Deirmendjian, D. (1964) Scattering and Polarization Properties of Water Clouds and Hazes in the Visible and IR, Appl. Opt. 3, 187-196.

Dubisch, R. (1974) On the Averaging of Ratios of Specific Heats in a Multi-component Planetary Atmosphere, Icarus 22, 474-475.

Elliot, J. L., Wasserman, L. H., Veverka, J., Sagan, C. and Liller, W. (1974) The Occultation of β Scorpii by Jupiter II. The Hydrogen/Helium Abundance in the Jovian Atmosphere, Astrophys. J. 190, 719-729.

Encrenaz, Th., Gautier, D., Michel, G., Zeau, Y., Lecacheux, J., Vapillon, L., and Combes, M. (1976) Airborne Interferometric Measurement of the Infrared Spectrum of Jupiter from 6 - 14 μm, Icarus 29, 311-314.

Erickson, E.F., Goorvitch, O., Simpson, J.P., and Strecker, D.W. (1978) Far Infrared Spectrophotometry of Jupiter and Saturn, Icarus 35, 61-73.

Fink, U. and Belton, M. J. S. (1969) Collision-Narrowed Curves of Growth for H_2 Applied to New Photoelectric Observations of Jupiter, J. Atmos. Sci. 26, 952-962.

Gillett, F. C. and Forest, W. J. (1974) Jupiter: Identification of Ethane and Acetylene, Astrophys. J. 187, L37-L40.

Gillett, F. C., Low, F. J. and Stein, W. A. (1969) The 2.8 - 14 Micron Spectrum of Jupiter, Astrophys. J. 157, 925-934.

Gillett, F. C. and Rieke, G. H. (1977) 5 - 20 Micron Observations of Uranus and Neptune, Ap. J. 218, L141-L144.

Giver, L. P. (1978) Intensity Measurements of the CH_4 Bands in the Region 4350Å to 10,000Å, J.S.Q.R.T. 19, 311 - 322.

Gopal, E. S. R. (1966) Specific Heats at Low Temperatures, Plenum Press, New York, 157 pp.

Gulkis, S., McDonough, T. R. and Craft, H. (1969) The Microwave Spectrum of Saturn, Icarus 10, 421-428.

Handbook of Chemistry and Physics, 42nd Ed., Chem. Rubber Co., Cleveland, Ohio.

Hansen, J. E. (1971) Multiple Scattering of Polarized Light in Planetary Atmospheres Part II: Sunlight Reflected by Terrestrial Water Clouds, J. Atmos. Sci. 28, 1400-1426.

Hansen, J. E. and Travis, L. D. (1974) Light Scattering in Planetary Atmospheres, Space Sci. Revs. 16, 527-610.

Harper, D. A., Low, F. J., Rieke, G. H. and Armstrong, K. R. (1972) Observations of Planets, Nebulae, and Galaxies at 350 Microns, Astrophys. J. 177, L21-L26.

Houck, J. R., Schaack, D., Reed, R. A., Pollack, J. and Summers, A. (1975) Jupiter: Its Infrared Spectrum From 16 to 40 Microns, Science 189, 720-722.

Irvine, W. M. and Pollack, J. B. (1968) Infrared Optical Properties of Water and Ice Spheres, Icarus 8, 324-360.

Joyce, R.R., Pilcher, C.B., Cruikshank, D.P., Morrison, D.(1977) Evidence for Weather on Neptune I, submitted to Ap.J.; abstract in B.A.A.S. 9, No.3, 471.

Kawata, Y. and Hansen, J. E. (1976) Circular Polarization of Sunlight Reflected by Jupiter, In Jupiter, ed. Gehrels, T., University of Arizona Press, 516-530.

Khanna, R., Boese, R. W. and Silvaggio, P. M. (1974) Abstract, Proceedings of Colloquium on Chemical Evolution of the Giant Planets, p. 33.

Khare, B. N. and Sagan, C. (1973) Red Clouds in Reducing Atmospheres, Icarus 20, 311-321.

Khare, B. N. and Sagan, C. (1975) Cyclic Octatomic Sulfur: A Possible Infrared and Visible Chromophore in the Clouds of Jupiter, Science 189, 722-723.

Khrgian, A. Kh. (1961) Cloud Physics, Israel Prog. Sci. Trans., Jerusalem, 392 pp.

Lasker, B. (1963) Wet Adiabatic Model Atmospheres for Jupiter, Astrophys. J. 138, 709-719.

Low, F. J. (1965) Planetary Radiation at IR and Millimeter Wavelengths, Bull. Lowell Obs. 6, 184-187.

Low, F. J. (1966a) Observations of Venus, Jupiter and Saturn at $\lambda 20\mu$, Astron. J. 71, 391.

Low, F. J. and Davidson, A. W. (1969) The Thermal Emission of Jupiter and Saturn, Bull. Amer. Astron. Soc. 1, 200.

Low, R. J., Rieke, G. H. and Armstrong, K. R. (1973) Ground Based Observations at 34 Microns, Astrophys. J. 183, L105-L110.

Lutz, B.L., Owen, T., Cess, R.D. (1976) Laboratory Band Strengths of Methane and their Application to the Atmospheres of Jupiter, Saturn, Uranus, Neptune, and Titan, Astrophys. J. 203, 541- 551.

Macy Jr., W., Gelfand, Jack and Smith, Wm. Hayden (1978) Interpretation of the 6818.9 Å Methane Line in Terms of Inhomogeneous Scattering Models for Uranus and Neptune, Icarus 34, 20-27.

Margolis, J. S. and Hunt, G. E. (1973) On the Level of H_2 Quadrupole Absorption in the Jovian Atmosphere, Icarus 18, 593-598.

Mason, H. P. (1970) The Abundance of Ammonia in the Atmosphere of Jupiter, Astrophys. and Space Sci. 7, 424-436.

Munch, G. and Spinrad, H. (1963) On the Spectrum of Saturn, Mem.Soc.Roy.Sci. Liege Series 5, 7, 541-542.

Murphy, R. E., Cruikshank, D. P., and Morrison, D. (1972) Albedos, Radii, and Temperature of Iapetus and Rhea, abstracted in B.A.A.S. 4, p. 367; 3rd Annual Meeting AAS Div. for Planetary Sciences, Kina, Hawaii.

Murphy, E. E. and Trafton, L. M. (1974) Evidence for an Internal Heat Source in Neptune, Astrophys. J. 193, 253-256.

Orton, G. S. (1975a) The Thermal Structure of Jupiter II. Observations and Analysis of 8 - 14 Micron Radiation, Icarus 26, 142-158.

Orton, G. S. (1975b) Spatially Resolved Absolute Spectral Reflectivity of Jupiter: 3390-8400 Å, Icarus 26, 159-174.

Owen, T. (1967) On the Abundance of Ethane in the Atmospheres of Jupiter and Saturn, Icarus 6, 138-139.

Owen, T. (1969) The Spectra of Jupiter and Saturn in the Photographic Infrared, Icarus 10, 355-364.

Owen, T. (1971) The 5520 Å Band of Ammonia in the Spectrum of Jupiter, Astrophys. J. 164, 211-212.

Poll, J. D. (1971) Estimate of the H_2 Abundance in the Atmosphere of Uranus from the Pressure-Induced Spectrum, In C. Sagan, T. C. Owen, and H. J. Smith (eds.), Planetary Atmospheres, IAU Symp. 40, Springer-Verlag, New York, 384-391.

Pollack, J. B. (1969) A Nongray CO_2 - HO_2 Greenhouse Model of Venus, Icarus 10, 301-313.

Pollack, J. B. and Ohring, G. (1973) A Numerical Method for Determining the Temperature Structure of Planetary Atmospheres, Icarus 19, 34-42.

Rieke, G. H. and Low, F. J. (1974) IR Measurements of Uranus and Neptune, Ap. J. 193, L147-L148.

Sagan, C. (1969) Gray and Nongray Planetary Atmospheres Structure, Convective Instability, and Greenhouse Effect, Icarus 10, 290-300.

Sagan, C. and Pollack, J. B. (1967) Anisotropic Nonconservative Scattering and the Clouds of Venus, J. Geophys. Res. 72, 469-477.

Sagan, C. and Salpeter, E. E. (1976) Particles, Environments and Hypothetical Ecologies in the Jovian Atmosphere, Astrophys. J. Suppl. 32, 737-755.

Silvaggio, P. M. (1977) Experimental Determination of Molecular Absorption Coefficients for Methane and Ammonia at Low Temperatures and Model Atmospheres for the Major Planets, Cornell University Report, CRSR 677.

Taylor, F. W. (1973) Preliminary Data on the Optical Properties of Solid Ammonia and Scattering Parameters for Ammonia Cloud Particles, J. Atmos. Sci. 30, 677-683.

Trafton, L. M. (1965) Unpublished Ph.D. Thesis, California Institute of Technology.

Trafton, L. M. (1967) Model Atmospheres of the Major Planets, Astrophys. J. 147, 765-781.

Trafton, L. M. (1971) A Semiempirical Model for the Mean Transmission of a Molecular Band and Application to the 10 μ and 16 μ Bands of NH_3, Icarus 15, 27-38.

Trafton, L. M. (1974) In "The Atmosphere of Uranus," NASA Ames Research Center, Moffett Field, California, 194 p.

Wickramasinghe, N. C. (1973) Light Scattering Functions for Small Particles, Wiley, New York, 506 p.

Wilholt, J. (1971) Handbook of Vapor Pressures, American Petroleum Institute Research Project 44, New York.

Woodman, J., Trafton, L. M. and Owen, T. (1977) The Abundances of Ammonia in the Atmospheres of Jupiter, Saturn and Titan, Icarus 32, 314-320.

Woodman, J. H., Trafton, L., and Owen, Tobias (1977) The Abundances of Ammonis in the Atmospheres of Jupiter, Saturn, and Titan, Icarus 32, 314-320.

Zemansky, D. (1957) Heat and Thermodynamics, McGraw-Hill, 390 pp.

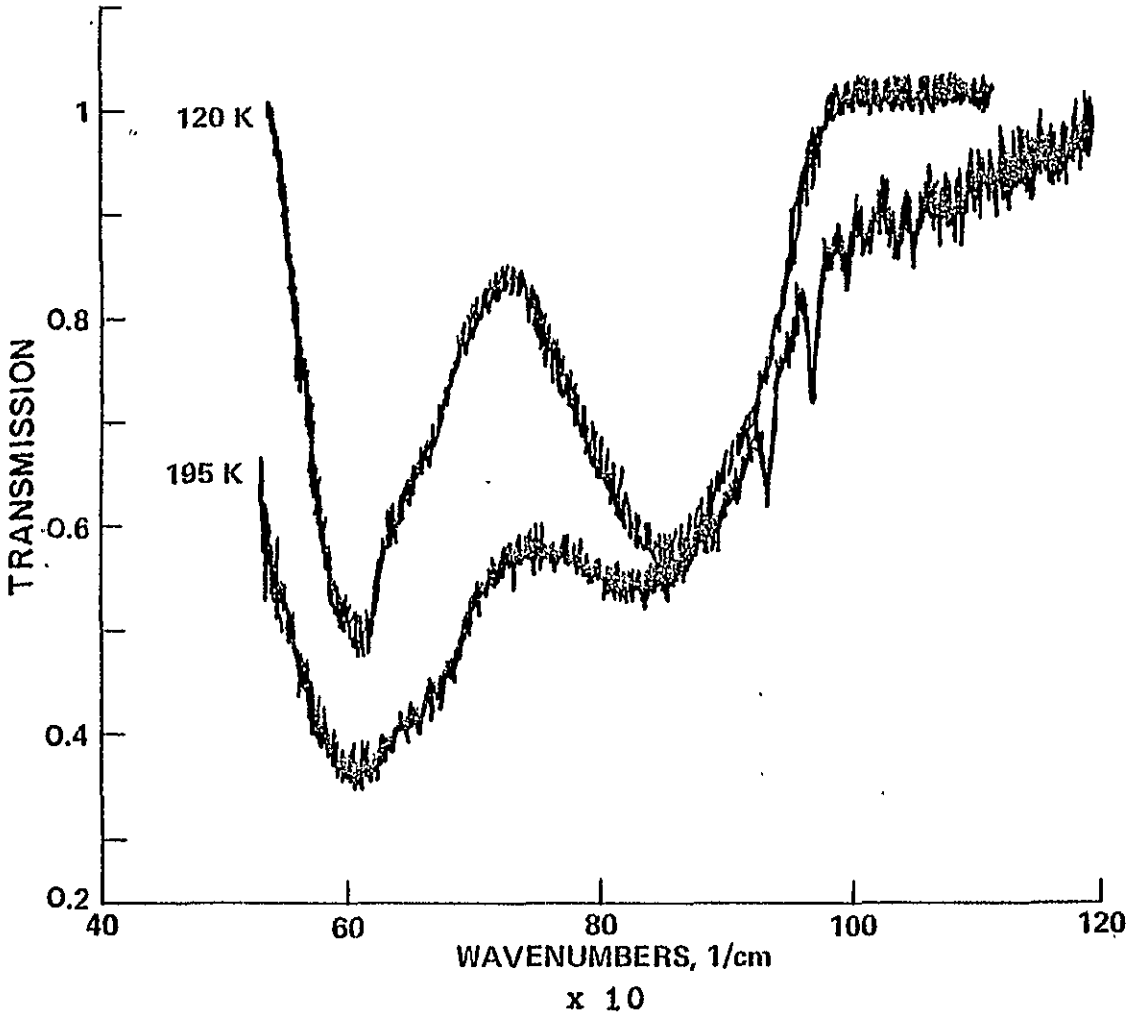
120 K
195 K
TRANSMISSION
1
0.8
0.6
0.4
0.2
40
60
80
100
120
WAVENUMBERS, 1/cm
x 10

Figure 1

WATANABE et al (1971)
CALCULATED VALUES
x 10⁻¹²
8
4
0
0
$\tilde{A}(\nu)/\rho^2$ (Amagat^{-2})
300 K
195
85
7500
8000
8500
9000
9500
FREQUENCY, cm^{-1}

Figure 2

JAMES E. HANSEN AND LARRY D. TRAVIS (1974)

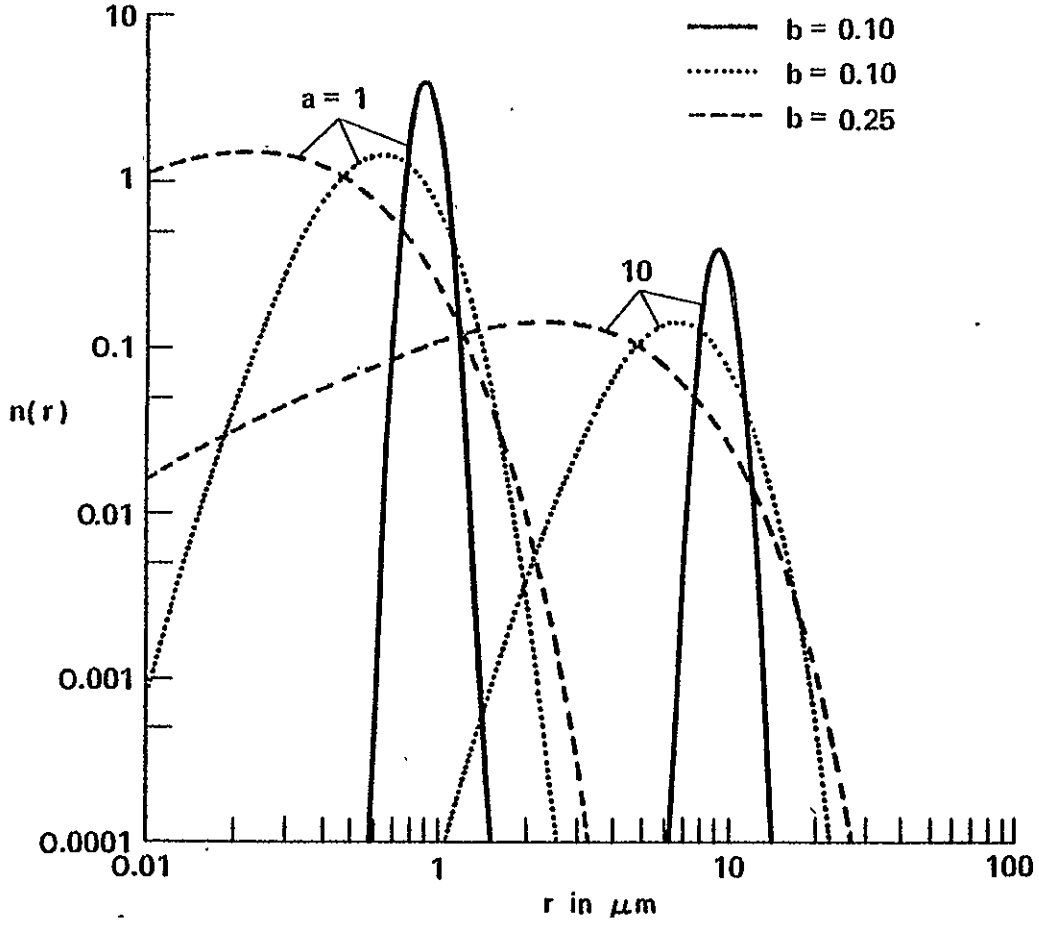

Figure 3

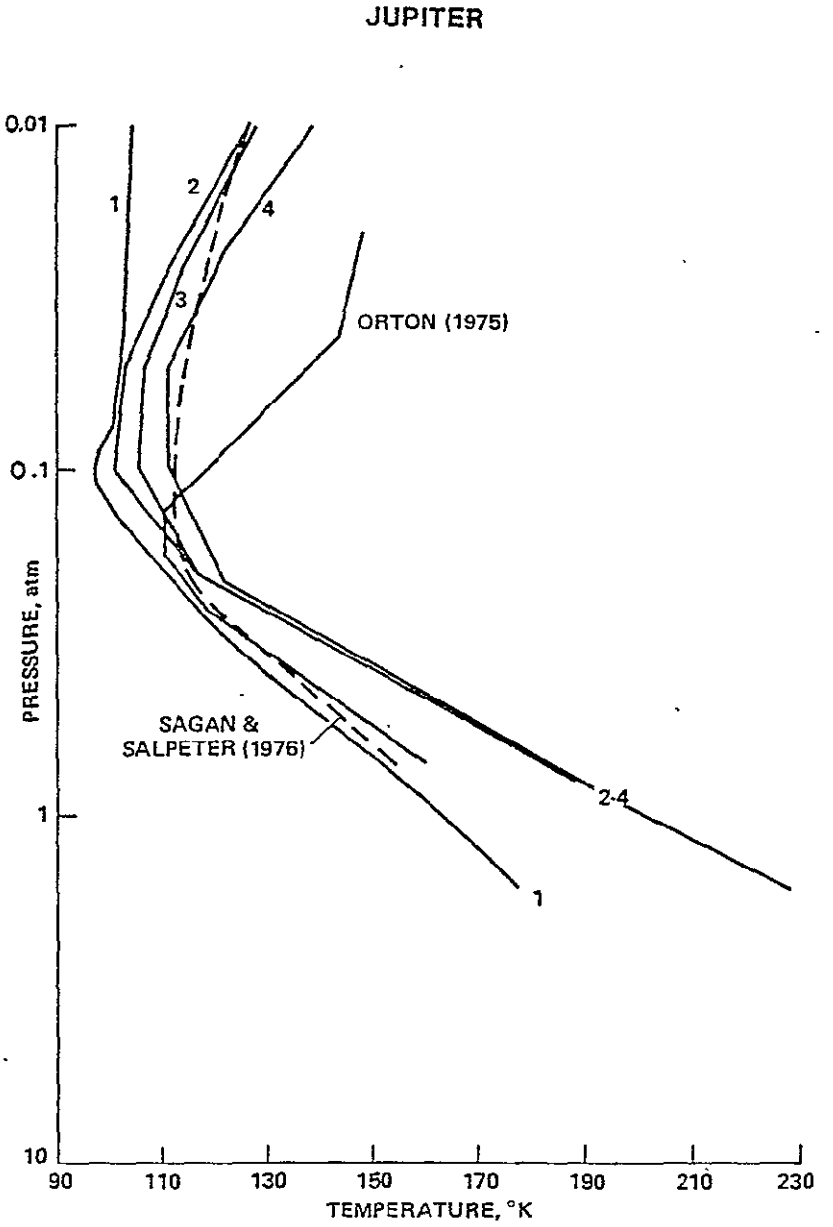
JUPITER
0.01
0.1
1
10
PRESSURE, atm
1
2
3
4
ORTON (1975)
SAGAN &
SALPETER (1976)
2-4
1
90
110
130
150
170
190
210
230
TEMPERATURE, °K

Figure 4

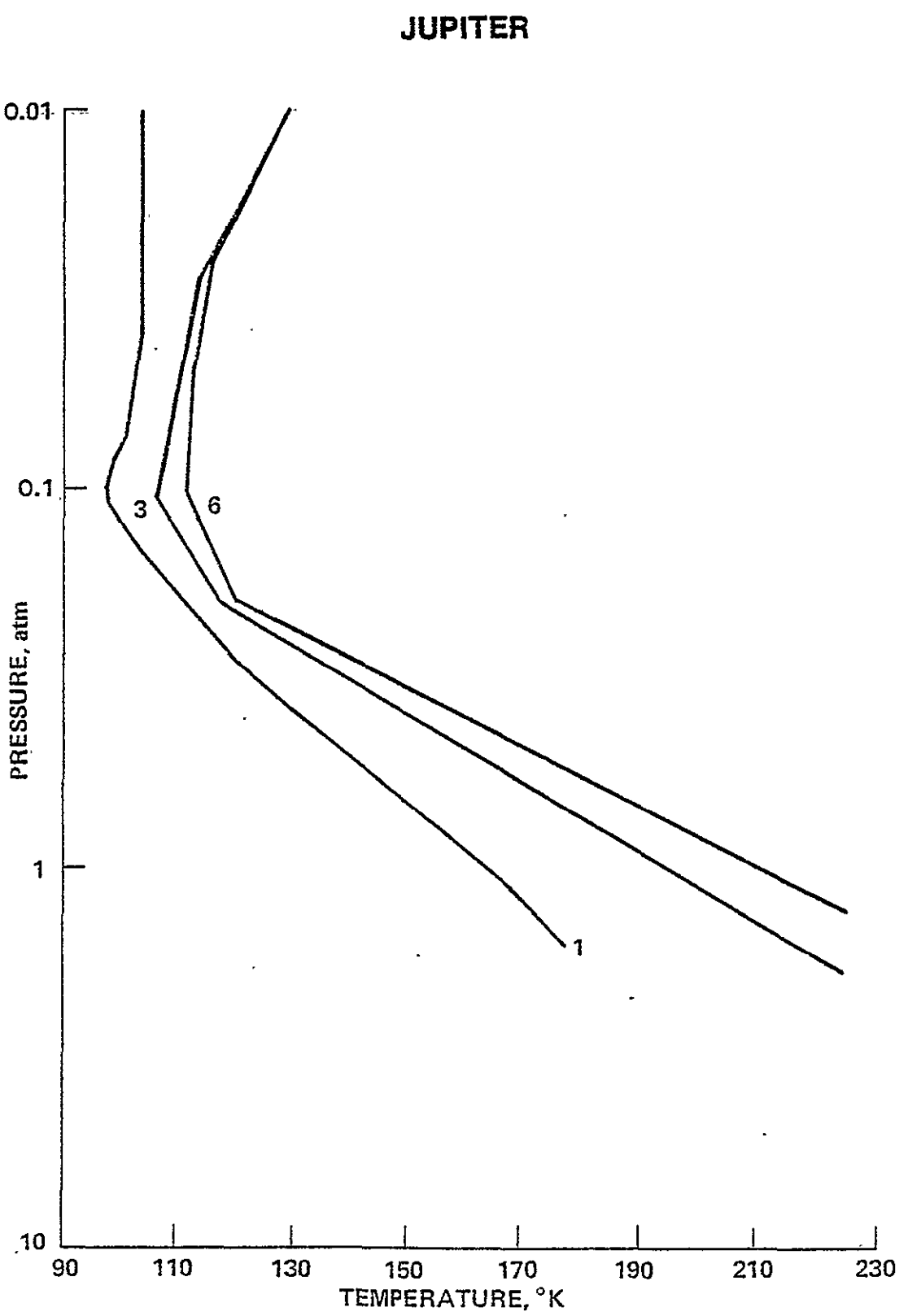
JUPITER
0.01
0.1
1
10
PRESSURE, atm
3
6
1
90
110
130
150
170
190
210
230
TEMPERATURE, °K

Figure 5

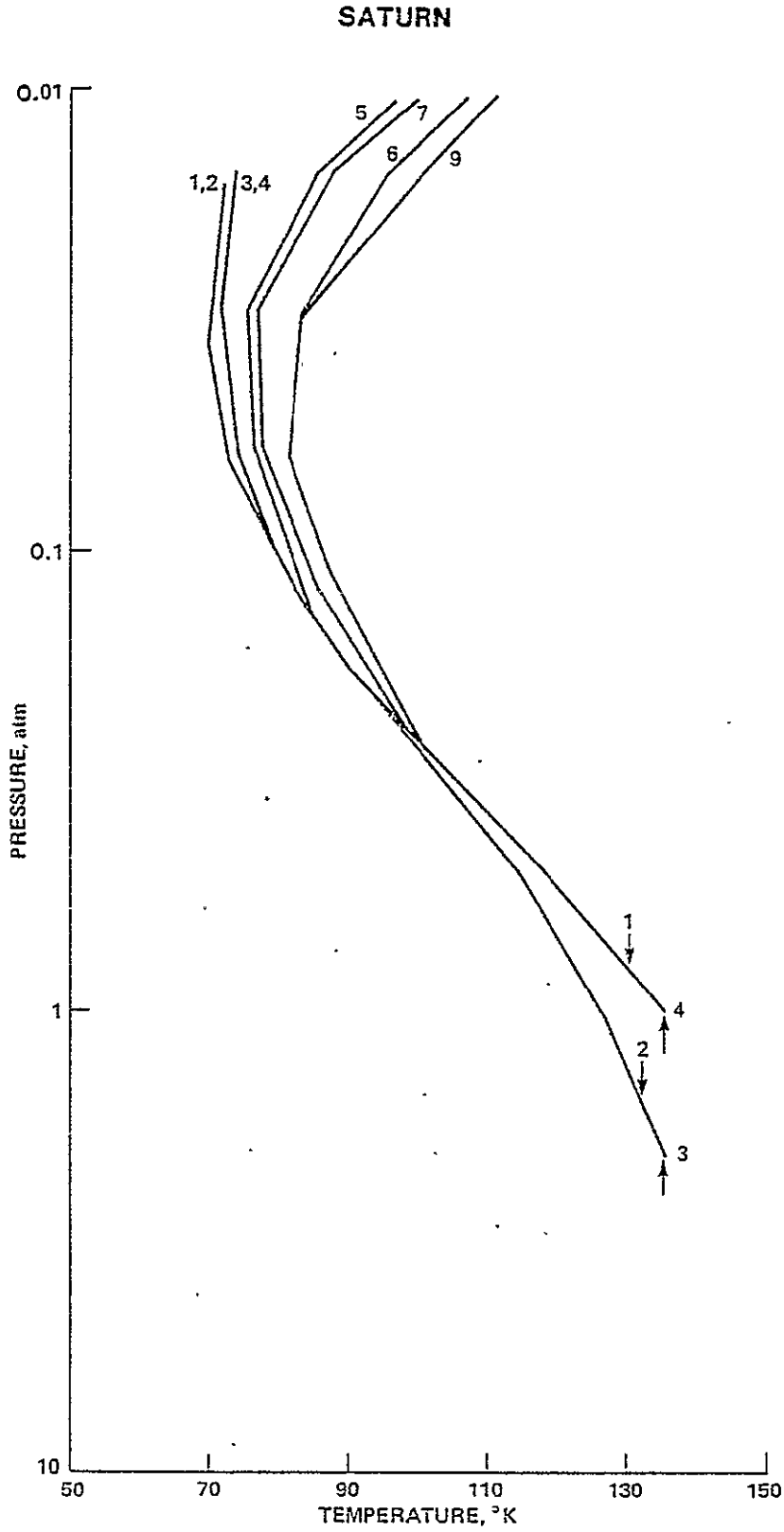
SATURN
0.01
0.1
1
10
PRESSURE, atm
50
70
90
110
130
150
TEMPERATURE, °K
1,2
3,4
5
6
7
9
1
2
3
4

Figure 6

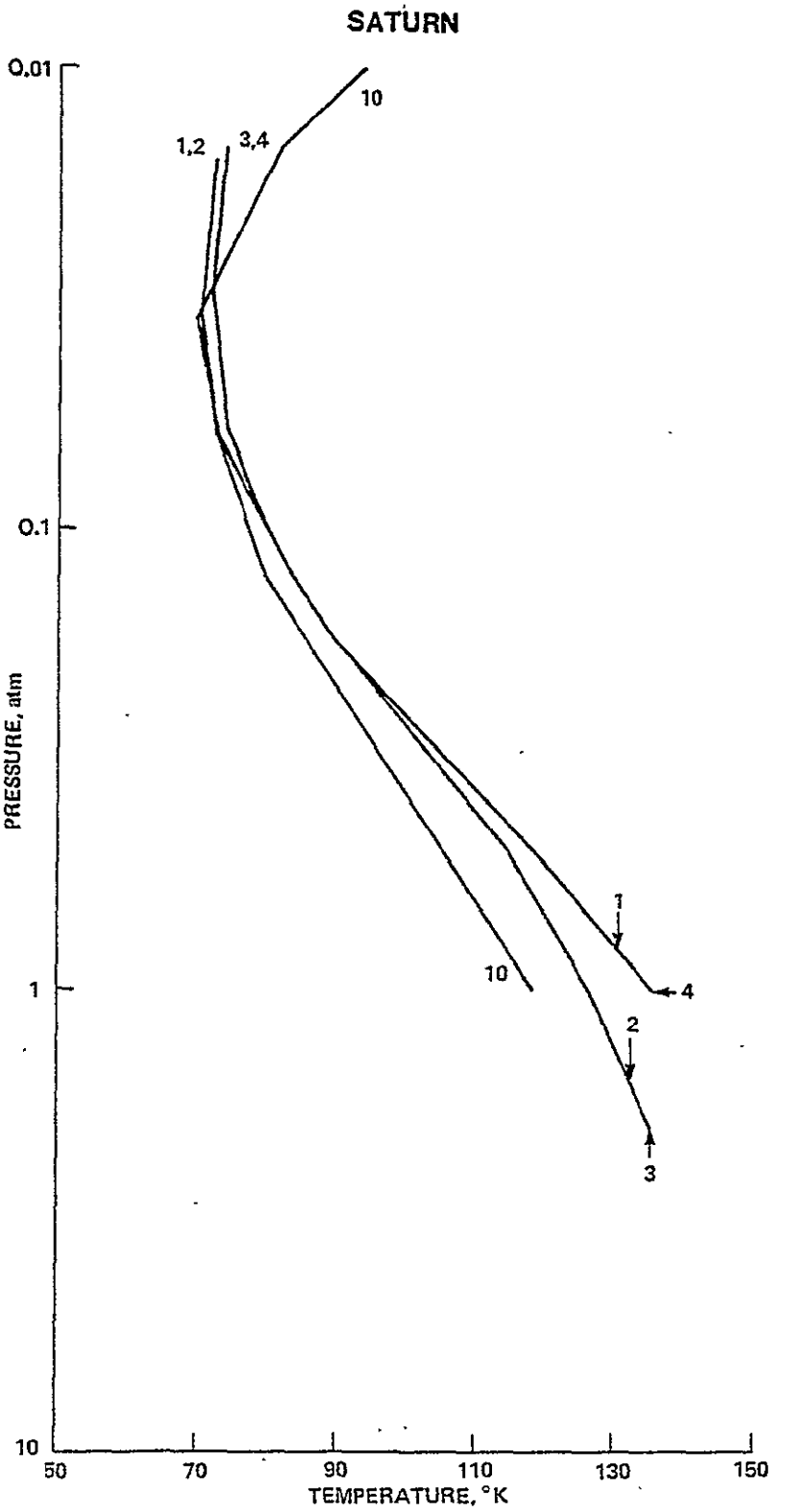
SATURN
0.01
0.1
1
10
PRESSURE, atm
1,2
3,4
10
10
1
4
2
3
50
70
90
110
130
150
TEMPERATURE, °K

Figure 7

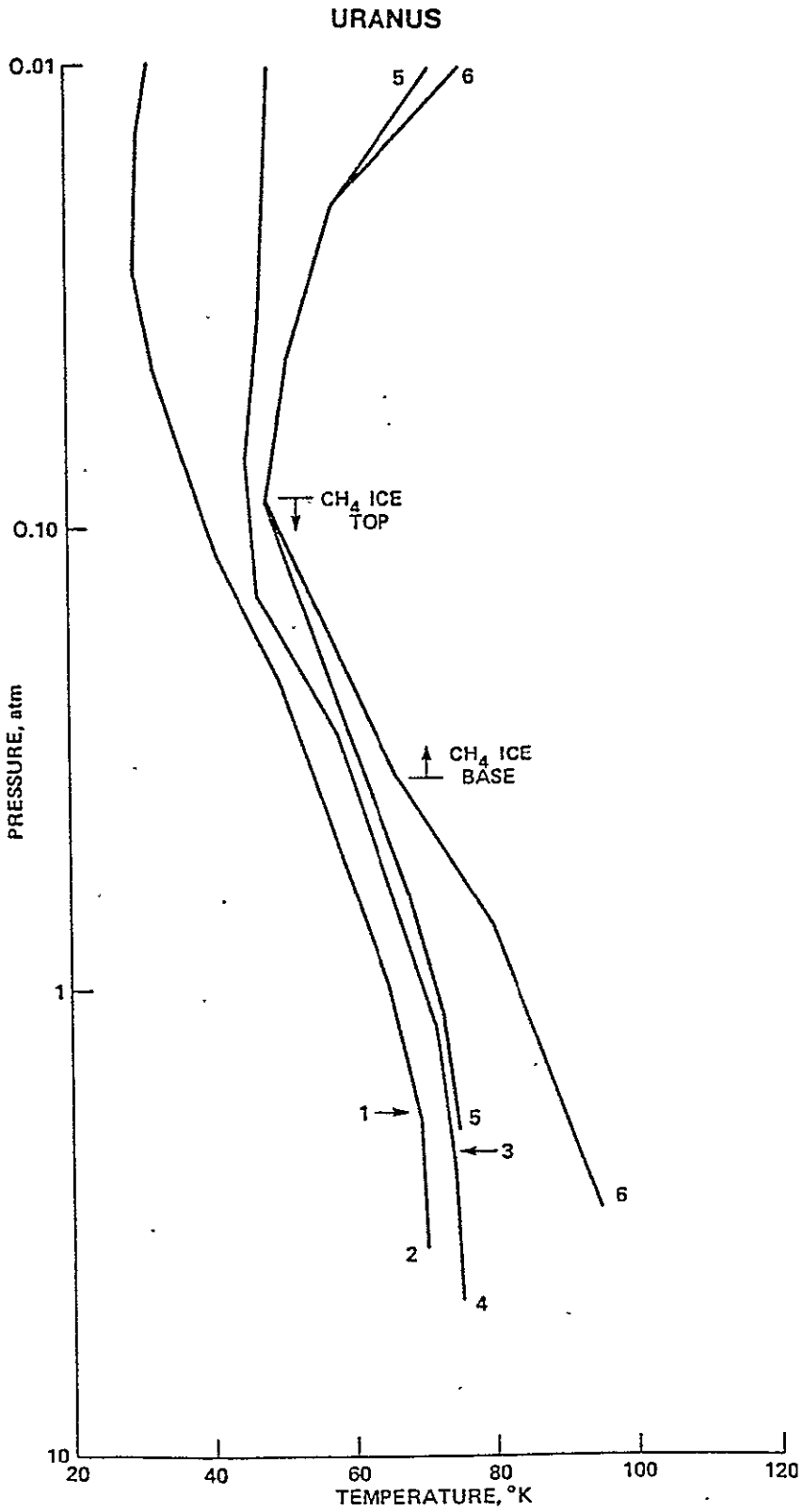
URANUS
0.01
0.10
1
10
PRESSURE, atm
5
6
CH4 ICE TOP
CH4 ICE BASE
1
5
3
6
2
4
20
40
60
80
100
120
TEMPERATURE, °K

Figure 8

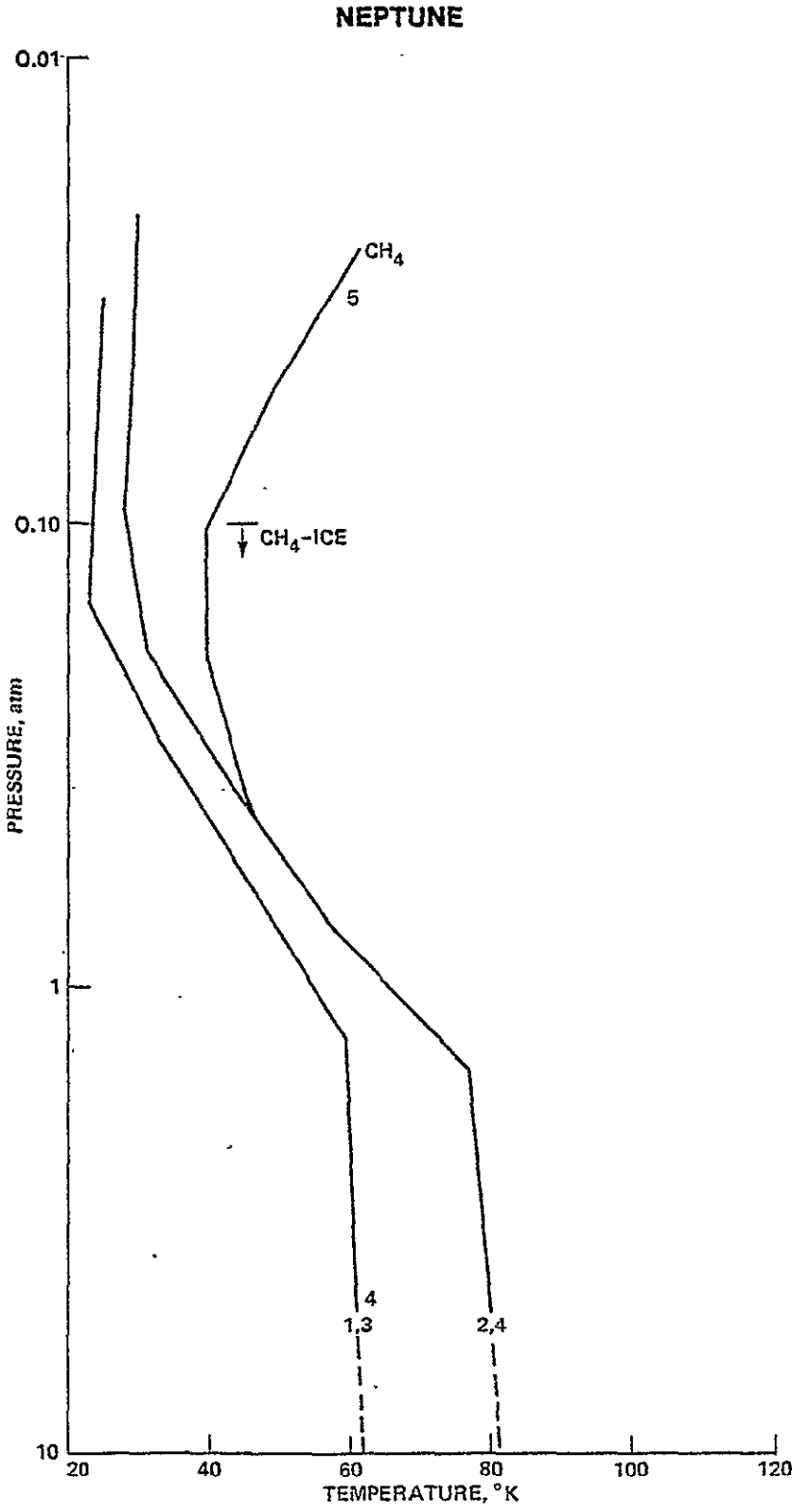
NEPTUNE
0.01
0.10
1
10
PRESSURE, atm
CH4
5
CH4-ICE
4
1,3
2,4
20
40
60
80
100
120
TEMPERATURE, °K

Figure 9

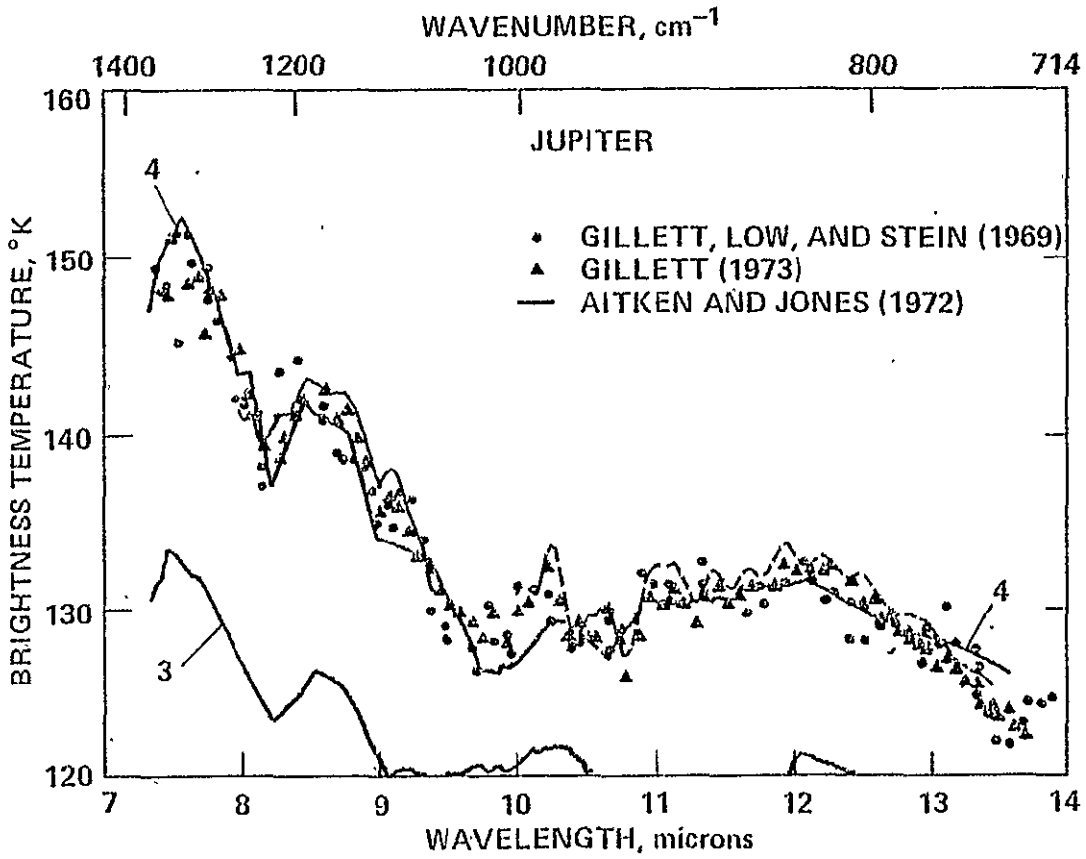
WAVENUMBER, cm^{-1}
1400
1200
1000
800
714
160
150
140
130
120
BRIGHTNESS TEMPERATURE, °K
JUPITER
GILLETT, LOW, AND STEIN (1969)
GILLETT (1973)
AITKEN AND JONES (1972)
4
3
4
7
8
9
10
11
12
13
14
WAVELENGTH, microns

Figure 10

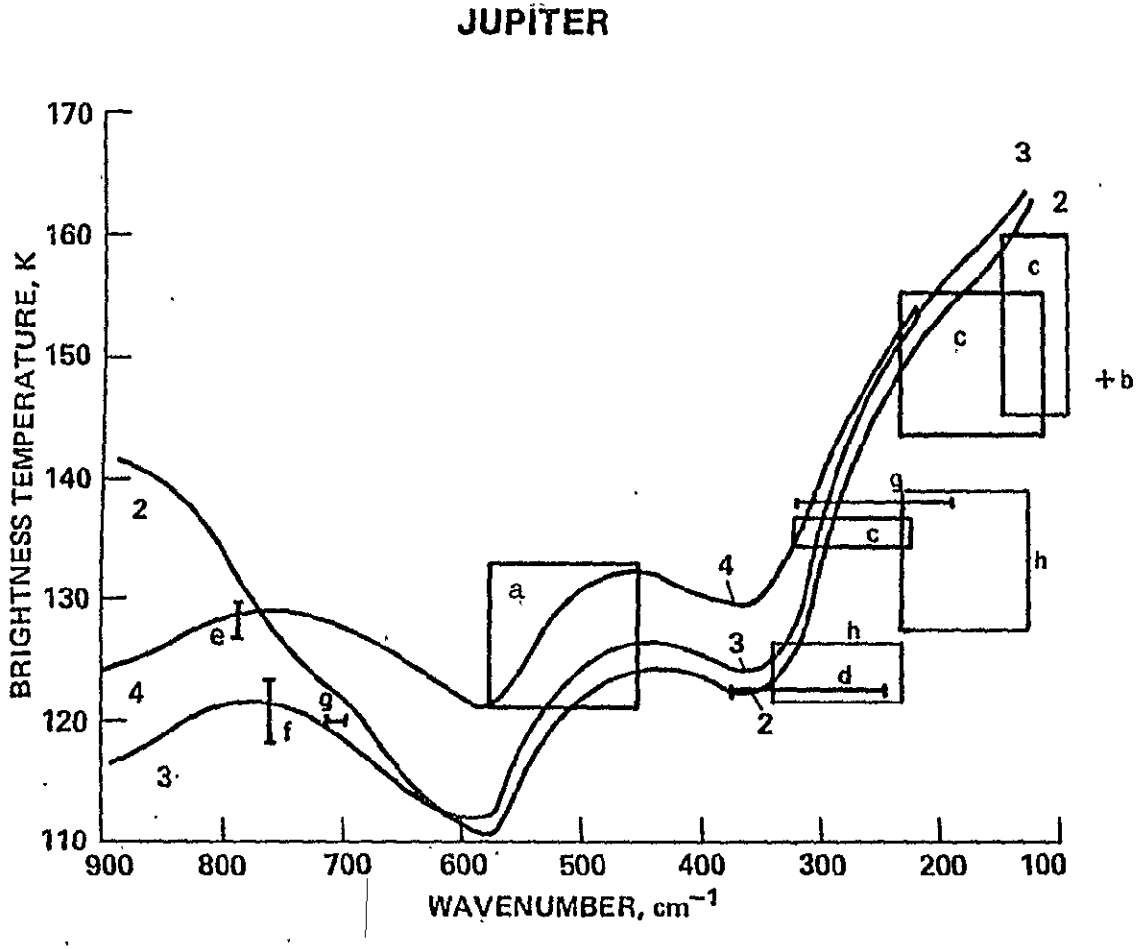
JUPITER
BRIGHTNESS TEMPERATURE, K
170
160
150
140
130
120
110
900
800
700
600
500
400
300
200
100
WAVENUMBER, cm⁻¹
a
b
c
d
e
f
g
h
2
3
4

Figure 11

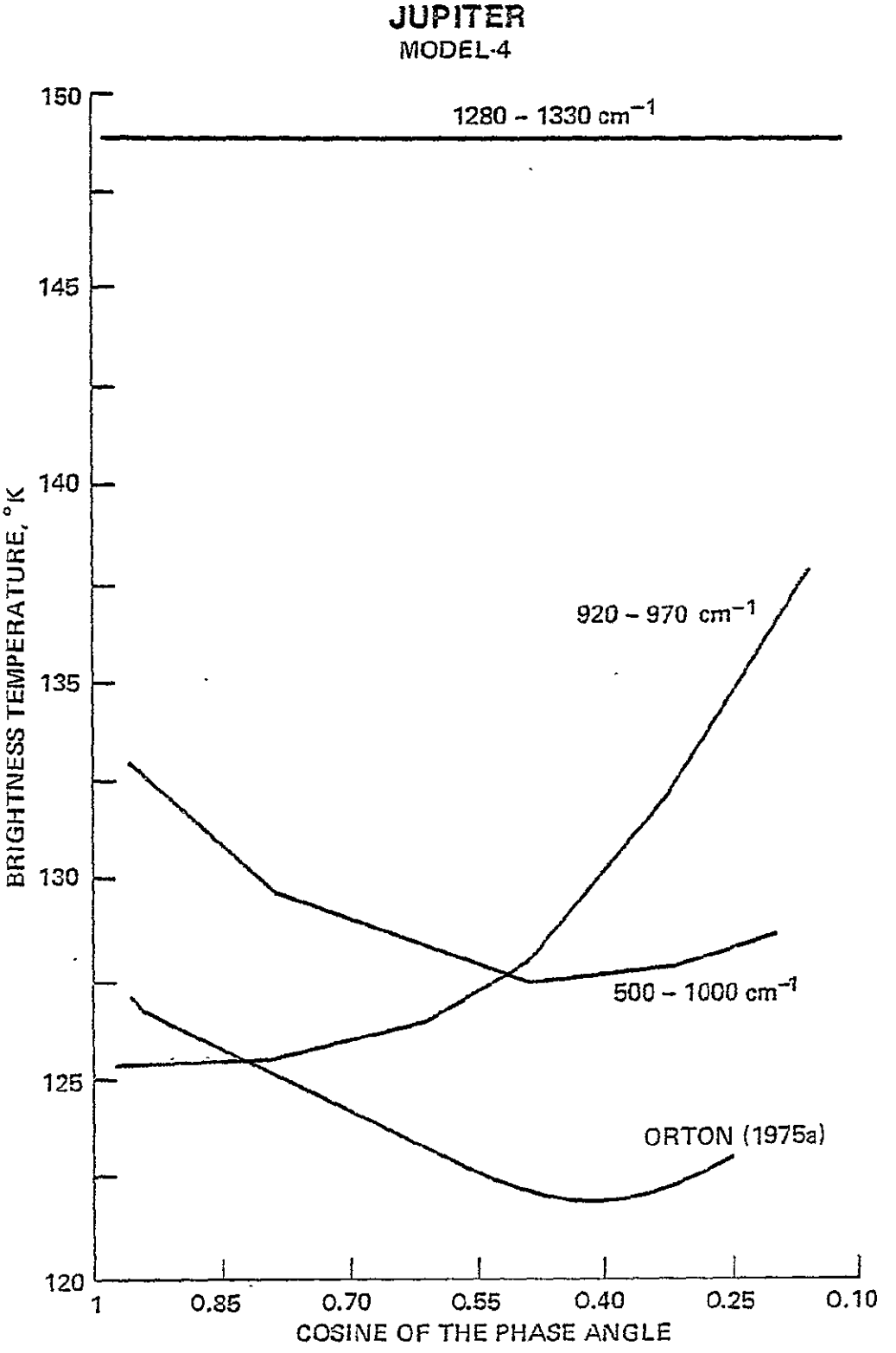
JUPITER
MODEL-4
1280 – 1330 cm^{-1}
920 – 970 cm^{-1}
500 – 1000 cm^{-1}
ORTON (1975a)
BRIGHTNESS TEMPERATURE, °K
150
145
140
135
130
125
120
1
0.85
0.70
0.55
0.40
0.25
0.10
COSINE OF THE PHASE ANGLE

Figure 12

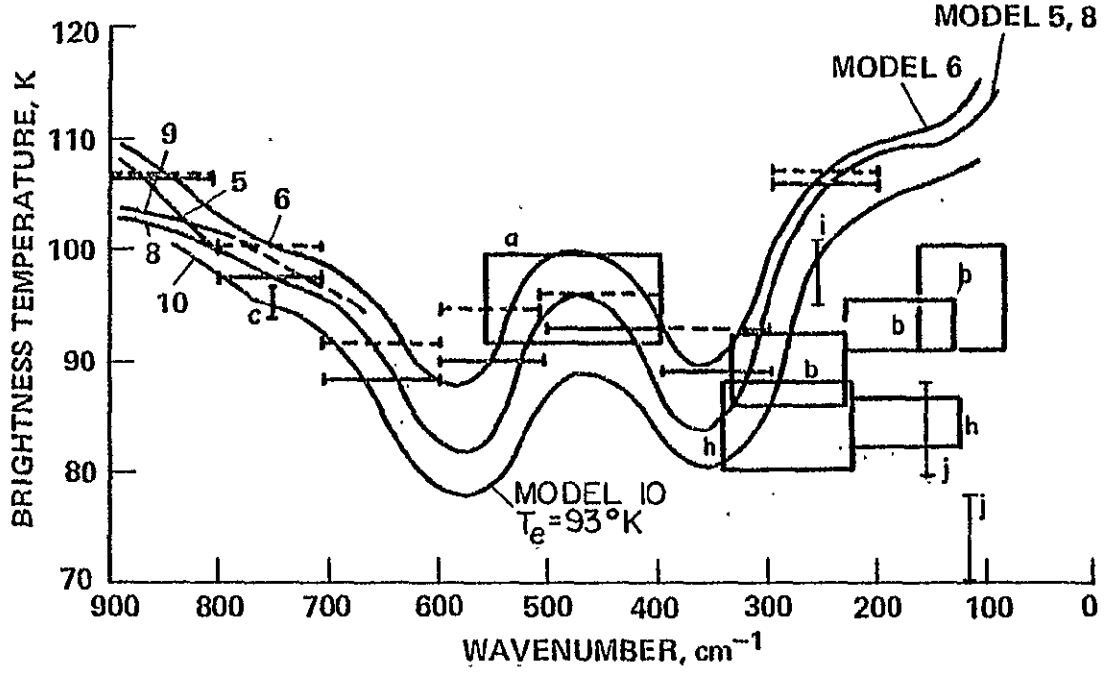
SATURN
MODEL 5, 8
MODEL 6
MODEL 10
T_e=93°K
BRIGHTNESS TEMPERATURE, K
WAVENUMBER, cm^{-1}
120
110
100
90
80
70
900
800
700
600
500
400
300
200
100
0
9
5
6
8
10
c
a
b
h
j

Figure 13

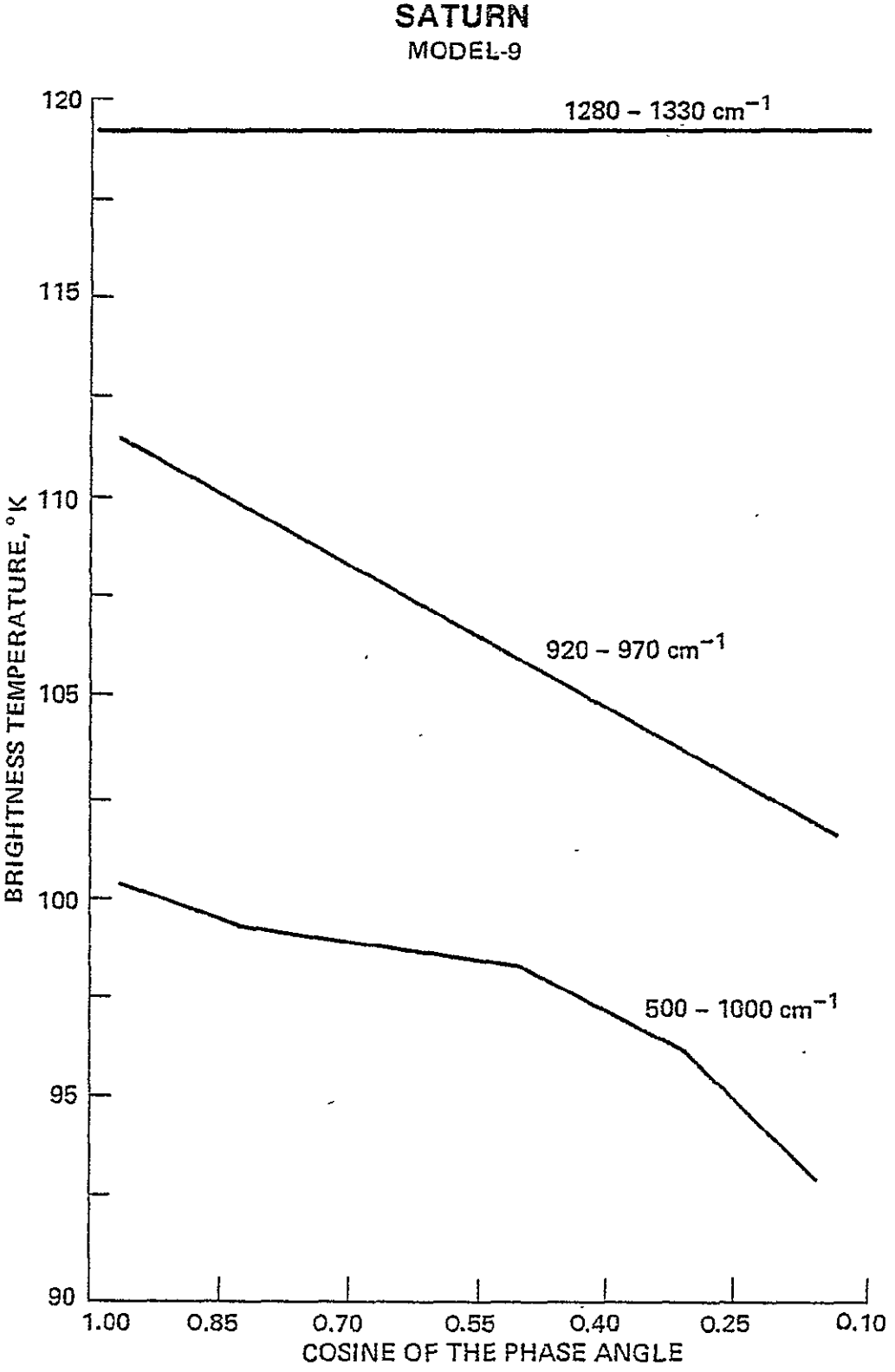
SATURN
MODEL-9
1280 – 1330 cm^{-1}
920 – 970 cm^{-1}
500 – 1000 cm^{-1}
BRIGHTNESS TEMPERATURE, °K
120
115
110
105
100
95
90
1.00
0.85
0.70
0.55
0.40
0.25
0.10
COSINE OF THE PHASE ANGLE

Figure 14

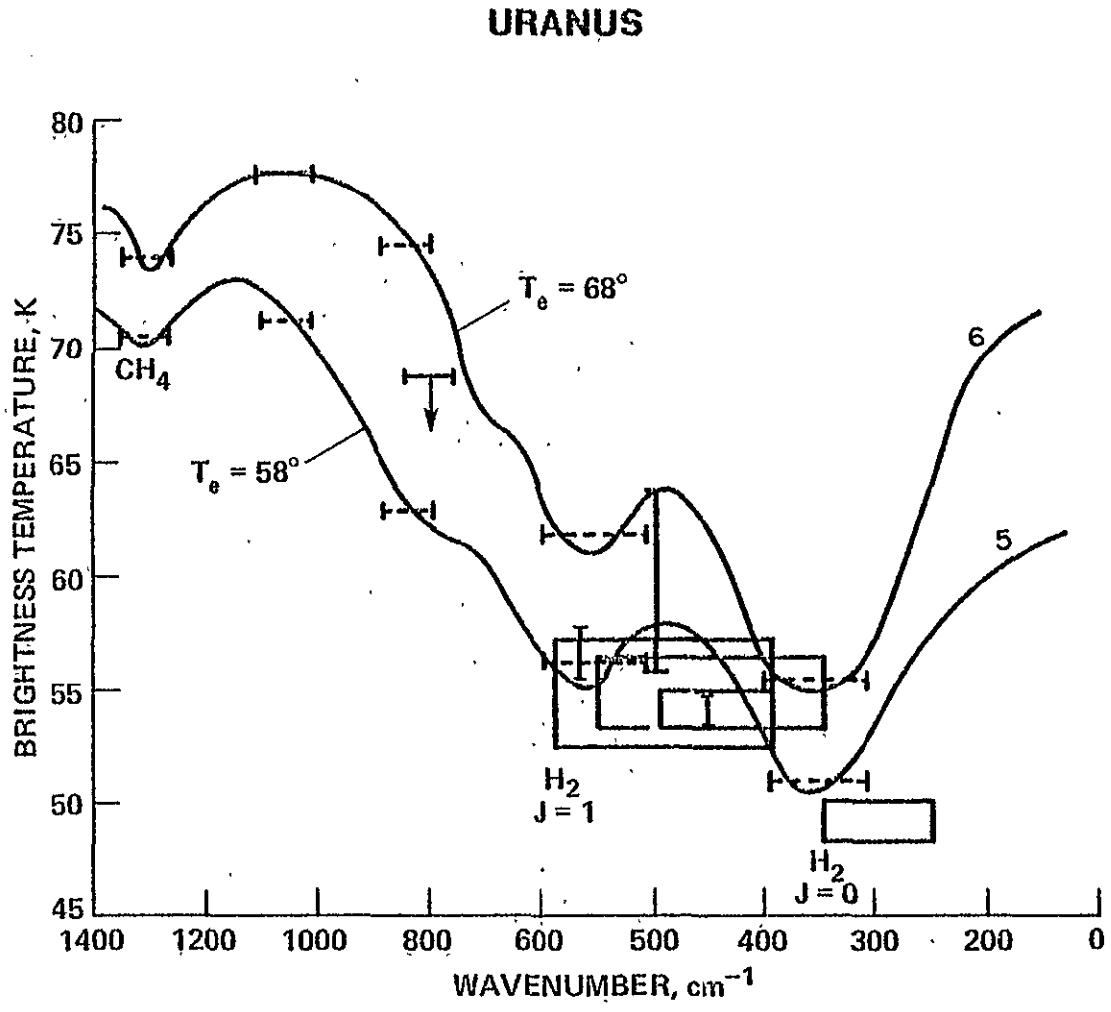
URANUS
BRIGHTNESS TEMPERATURE, K
80
75
70
65
60
55
50
45
1400
1200
1000
800
600
500
400
300
200
0
WAVENUMBER, cm^{-1}
T_e = 68°
T_e = 58°
CH_4
6
5
H_2
J = 1
H_2
J = 0

Figure 15

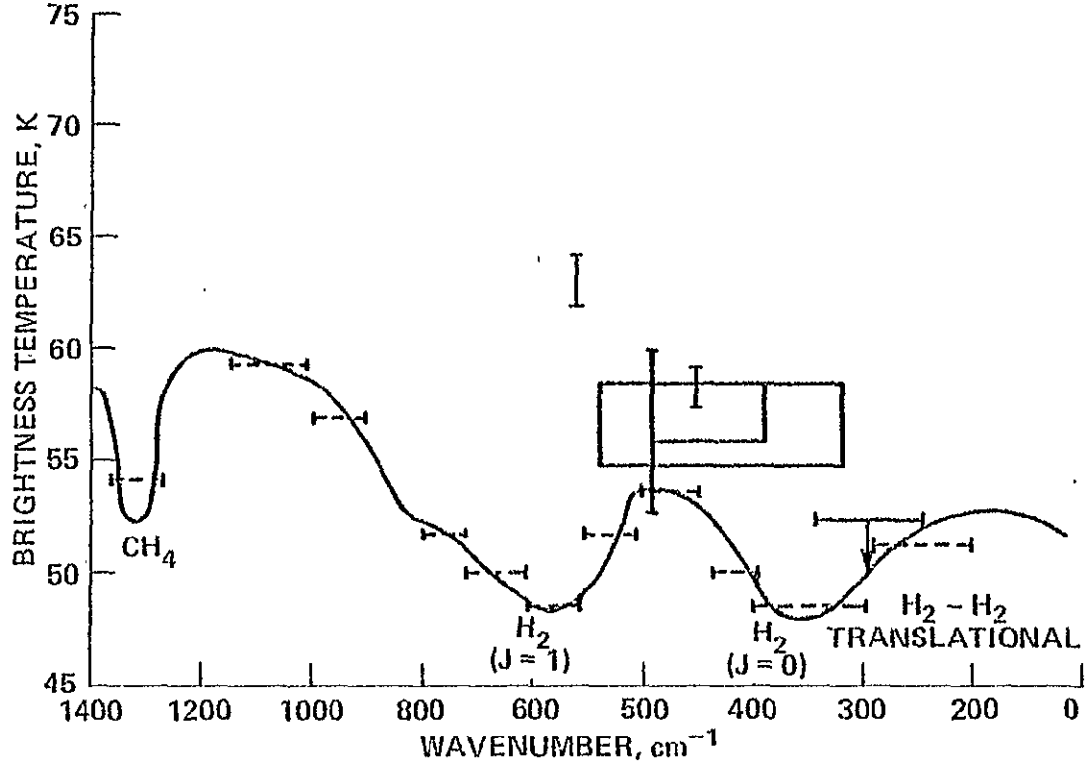
NEPTUNE
BRIGHTNESS TEMPERATURE, K
75
70
65
60
55
50
45
1400
1200
1000
800
600
500
400
300
200
0
WAVENUMBER, cm^{-1}
CH_4
H_2
(J = 1)
H_2
(J = 0)
$H_2 - H_2$
TRANSLATIONAL

Figure 16